22nd IAEA Fusion Energy Conference
Geneva, October 2008

Summary of contributions on Fusion Technology and ITER Activities

D.Stork
Euratom-UKAEA Fusion Association,
Culham Science Centre, Oxfordshire OX14 3 DB, United Kingdom

1 **Introduction**

This summary paper reviews those contributions to the 22nd IAEA Fusion Energy Conference (FEC) selected under the categories of Fusion Technology (FT), ITER Activities (IT) and Safety and Economic Studies (SE). The IT category was limited to those papers put forward officially by the ITER Organisation (IO). In addition, several papers in the FT category featured ITER-related work.

In the Fusion Technology category 68 papers were split amongst the areas of:
- new 'Fusion Research Machines' – 12 papers;
- 'Plasma Engineering' (Heating and Current Drive systems, Diagnostics, Control) – 14 papers, including ITER-related work;
- Plasma Facing Component (PFC) Materials and Divertor Technology – 9 papers including ITER-related work;
- Radiation properties and Activation of Materials – 8 papers;
- Blankets/Fuel Cycle – 10 papers, mainly based on ITER Test Blanket Module (TBM) studies;
- Reactor design – 11 papers;
- Safety – 2 papers;
- Remote Handling - 1 paper; and
- Fuelling – 1 paper.

Apart from the FT papers dealing with ITER-related work, there were 57 papers submitted through IO on 'ITER activities' (21 of these are essentially 'Physics-based'). Finally only two papers were submitted in the SE category.

With such a wide-ranging selection, the reviewer has concentrated on those results which have more general import, and hence will not review each paper. This review paper is organised such that the new or planned Fusion Research Machines are discussed first, followed by the ITER Activities papers, incorporating relevant papers from the FT category in Heating and Current Drive and Diagnostic areas . Then in sequence the review covers: Divertor Technology and PFCs; Materials and Blanket Studies; Reactor Studies; and finally the Economics of Fusion.

2 **Fusion Research Machines**

This category included contributions from machines which have started operation since

the 21st IAEA FEC, which I will term 'new born', from machines under construction, and proposals for new devices.

2.1 *New born machines*

Two new tokamak machines announced first plasma operation at this conference, the Korean KSTAR device [1] and the Japanese QUEST [2]. They represent two different strands of tokamak research, with KSTAR having an aspect ratio typical of the 'mainstream' (A=3.6), and QUEST being a spherical tokamak (ST) with a tight aspect ratio (A=1.7).

KSTAR is a medium-size tokamak (major radius R = 1.8m , minor radius a = 0.5m). It is the first tokamak to be constructed with superconducting coils of Nb_3Sn, with all toroidal field (TF) coils, and 10 of the 14 poloidal field (PF) coils fabricated from this material. The coil system is shown in figs 1(a) and 1(b). The TF system has been commissioned up to nearly half field (1.5T at the plasma axis, against a full performance of 3.5T), and plasma commissioning has progressed to achieve133 kA for 862 ms (see fig 1(c)). The impressively thorough commissioning, with the machine systems 94% available, was documented in several contributions [3] - [6]. This experience will be valuable for ITER.

QUEST has an eventual design goal of 0.3MA plasma current and is intended to operate as a steady-state ST with a current of 0.1 MA for over 100 s. It features an Electron Bernstein Wave (EBW) current drive system of 1 MW at 8.2 GHz, and will eventually have 2 MW of Neutral Beam Injection (NBI). It also has an all-metal (primarily tungsten) wall, eventually aimed at high temperature operation. The programme for 2008-09 will concentrate on plasma start-up studies.

2.2 *Machines in detailed design or construction*

Reports were presented on the design and construction of three very different machines for progressing Fusion Energy research. These were: the International Fusion Materials Irradiation Facility (IFMIF); the Wendelstein W-7X stellarator; and the KTM tokamak.

IFMIF is an accelerator-based neutron source for fusion material irradiation testing and the next phase (the so-called Engineering Validation and Engineering Design Activity – EVEDA) is now entered as a collaborative project under the Broader Approach programme between the European Union (EU) and Japan. IFMIF is regarded as one of the pillars of the 'Fast Track' programme for development of Fusion Power. The latest progress with the design was presented [7]. The main goal of the EVEDA is to deliver the detailed engineering design file of IFMIF by June 2013, and to validate the design, manufacture and test of three main prototypes: the low energy part of the accelerator (up to 9 MeV) at full current (125 mA); the lithium target at 1/3 scale; and the main components of the High Flux Test Modules,

including thermohydraulic tests and irradiation of full-size rigs. During 2008 the choice of superconducting technology was made for the Drift Tube Linac (DTL) par t of the accelerator. This is shown in fig 2. Key advantages leading to the choice of this technology were requirement for continuous working, shorter length and easier integration with focussing magnets. For the lithium target loop an erosion/corrosion test loop, Lifus3 was built and the erosion/corrosion properties of AISI 316 and Eurofer steels were tested, showing a better behaviour than martensitic steels. Removal and cleaning methods for atmospheric gases and tritium were evaluated and experiments on Li combustion were also completed. The surface properties of the hot traps with metallic Yttrium, used to remove tritium, and Titanium, used to remove nitrogen from the lithium were evaluated. Results in the 1-10 wppm impurities range were achieved, with pointers to surface and gettering treatments to improve these figures.

Wendelstein -7X is a fully-optimised low-shear stellarator of the Helias type with NbTi superconducting coils under construction at Greifswalsd in Germany. The construction has experienced a number of serious set-backs and considerable delays. The project has been completely re-organised and the new schedule is robust and construction is now on-schedule for first plasma in 2014 [8]. Manufacture and delivery of the NbTi coils (50 non-planar and 20 planar, each of about 3m diameter) is now well-advanced with 49 out of 70 coils successfully tested. All ten half-modules of the extremely complex cryostat are manufactured and ready for assembly. Amongst other progress, the high hat flux (HHF) divertor target elements, consisting of Carbon-fibre-composite (CFC) tiles electron-beam welded to Copper-chrome-zirconium (CuCrZr) base plates have been successfully tested to 8500 thermal cycles at 10 $MW.m^{-2}$.

Progress on the KTM tokamak programme was reported by the team from the National Nuclear Centre of Kazakhstan [9]. KTM is a medium-sized tokamak (R=0.9m, a =0.45m), relatively close to an ST configuration and is intended for material testing in a joint project between the Russian Federation and Kazakhstan. Its scientific programme includes tests of first-wall armour and divertor tiles; physics and technology of edge plasma and divertor diagnostics, control of fluxes to the divertor area; and mock-ups of divertor components using lithium capillary technologies. In addition it will study plasma heating with radio-frequency (RF) waves. First plasma operation is intended in 2010.

2.3 New machine proposals

Two new proposals were presented for tokamaks to be built in the timeframe of the ITER programme. These machines are aimed to address various parts of the missions which are relevant to an 'ITER generation' machine. To be compatible with a 'Fast Track' view, the relevant issues should ideally all have relevance to a DEMO device. A list of such issue not fully-addressed by ITER itself would be:

- long-pulse 'industrial-level' reliability of H&CD systems;
- high efficiency current drive;

- high-β plasma operation and stability;
- extreme power, erosion-resistant high-temperature divertors (ITER changes a divertor out after ~0.08 full power years (fpy) – DEMO will need >2 fpy lifetime);
- operation with a hot wall (700°C).

The two machine designs presented were the Fusion Advanced Studies Torus (FAST) from the ENEA Frascati group [10], and the National High Power Advanced Torus Experiment (NHTX) from the US PPPL Princeton group [11]. Both machines aim to address DEMO divertor concepts, but FAST has an additional fast particle mission (not one of the priorities listed above).

A fairly detailed design of the FAST machine was presented. The device has conventional copper coils cooled to 30K by gaseous cold helium by encasing in a cryostat[12]. The pulse length is thus extended, although the coils are heated adiabatically within the pulsing period. The device is a high-field, medium-sized tokamak with a 'conventional' aspect ratio ~ 3 D-shaped plasma (R=1.82m, a =0.64m). The load assembly design is shown in fig 3(a). FAST is intended to operate up to plasma current, I_p = 6.5MA and TF, B_T = 7.5T, but at this level it will have a current flat top limited to 13s. This high field operation is intended for fast particle studies, with the fast ions being created from a minority-ion population by Ion Cyclotron Resonance Heating (ICRH) waves. The long-pulse programme for DEMO divertor studies can be carried out at 3MA/3.5T, where the device will have a steady conditions pulse-length of ~ 160s. The power loading to major radius figure of merit (P/R) will be ~ 22 $MW.m^{-1}$, putting it at the edge of the DEMO range. The main divertor will be made of tungsten monoblocks on actively-cooled copper substructure, and the divertor elements are intended to be replaced by remote handling (see fig 3(b)). There are also plans for a liquid-Lithium divertor, based on the experience from FTU tokamak (see section 4.1).

In contrast, NHTX is described as an 'existence proof design' by its proponents, based on the driving parameters which would be necessary to carry out a given DEMO-related programme. The concept (fig 4(a) and (b)) is based on a medium-size (R=1m) ST configuration with an aspect ratio of ~ 1.8, and a high elongation of 2.7-3.0. The design exploits the compact nature of the ST, and with 50 MW auxiliary heating (30 MW of NBI at 110 kV energy and 20 MW RF), it achieves a potential power loading figure of merit of P/R ~ 50 $MW.m^{-1}$ at the divertor. The NBI-current drive and bootstrap current are predicted to allow a pulse length in the range 200-100s at I_p=3.5MA and B_T = 2T. The ability of the ST to run at high normalised plasma pressure enables β_N = 4.5 to be predicted. The mission of the device calls for a hot first wall capability (1000K), in order to study the effects of hydrogenic retention in the metal (tungsten) walls at reactor-relevant temperatures. The pulse-length range is set by the need to exceed the times(~ 100 s) when the particle balance in a present device like Tore-Supra [13] is seen to come into equilibrium. In addition to tungsten divertors, liquid-Lithium concepts are also foreseen, and these would be tested in 'conventional' divertor configurations, such

as in fig 4(b), or expanded divertor configurations of the 'super-X' type (See fig 4(c))[14]. Calculations predict that this configuration, where the scrape-off layer flux surfaces are taken to larger radius and through a very low poloidal field region thus increasing the connection length to the divertor target, could reduce the target power loading for 50 MW input below 10 $MW.m^{-2}$, even in the absence of any divertor region radiation or the absorption in evaporated lithium.

3 ITER activities in physics and technology

There has been considerable progress in the design of ITER since the 21st FEC in 2006, and this was summarised in the overview paper on engineering system design [15]; and in summary contributions on safety and licensing [16] and physics activities [17]. Below we report on the details from the more significant IT and FT contributions which supported these summaries.

3.1 *Tokamak operations physics studies*

There has been a prolific activity for the ITER Design Review, and this activity was reported in many high-quality contributions at this conference. In particular in many cases, significant progress in many areas of basic plasma control and surface interaction physics has come from cross-machine collaboration. Amongst the areas which have been addressed are:

- plasma discharge control including start-up, flat-top and current decay;
- operational space and vertical stability issues in plasma control;
- ELM damage, control and mitigation;
- RWM control;
- disruption mitigation;
- first wall design; and
- experiments with TF ripple.

The experiments to determine the effect from TF ripple on thermal energy confinement, conducted on JET and JT-60, were covered by contributions in the EX category at the conference and are discussed in a parallel summary of those sessions. The remaining topics are covered below.

The time-development of ITER discharges in the reference I_p = 15 MA, 'Q=10' standard ELMy-H-mode scenario [15] was reported from collaborative multi-machine experiments on a number of existing tokamaks [18]. Specific experiments on ASDEX –Upgrade (AUG), C-mod, DIIID, JET and JT-60U, studied the various aspects of the evolution of models of the ITER reference discharge in the breakdown, current ramp-up, current flat-top and ramp-down phases. Plasma breakdown in the ITER conditions (field < 0.33 $V.m^{-1}$) was found to be possible in Ohmic conditions on JET and with Electron Cyclotron Resonance Heating (ECRH) assist on all machines. With the JET results, it is now no longer deemed necessary to provide a 127 GHz ECRH system for start-up on ITER. For the current ramp up

phase, the advantage of using a full-bore plasma shape is evident, with lower inductance ($l_i = 0.7 – 1.0$) and better density and impurity control. The large bore also aids early transition to X-point configuration and early heating to enter the H-mode and save volt-seconds (over 25% savings can be achieved). The range of l_i values achieved in the current rise phase on the various machines in this study is shown in fig 5 , where access to the H-mode clearly provides the best results. Feedback control of l_i using additional heating was achieved on several machines. A comparison of the start up phases in JET [18] and DIIID [19] is shown in fig 6. The collaborative programme also characterised the flat-top volt-seconds consumption and timescales for achievement of steady-state in density and temperature profiles after L-H transitions for both the reference discharge and the 'hybrid' variant [18]. The ramp-down phase studies show that the control of the ramp-rate on ITER is required to avoid high-inductance values and loss of plasma control. Preliminary studies in JET, ASDEX-U and DIID show that slow current ramp-down without additional flux-consumption from the poloidal field can be achieved with additional heating to keep the plasma in H-mode but, apart form the high levels of heating involved (>50% of that needed to keep an H-mode at full-field), the control of plasma density is difficult in the H-mode. The researchers conclude that more modelling and experimental simulation of the ITER decay-phase is urgently needed.

The multi-machine studies have informed and validated the successful design exercise to improve the machine operating space envelope for the 15 MA reference scenario [20]. By concentrating on the need to maintain a full-bore start-up and on the volt-seconds requirement to give the 400 s flat-top nominal burn-phase for the scenario, the necessary changes to PF and Central Solenoid (CS) currents and force limits were evaluated. Engineering substantiation [20] has shown that the changed limits can be accommodated by modest changes within the design or reference assumptions. With reference to fig 7(a), the design changes established are: 20-25% increase in current and field limits on the poloidal coils PF1- PF6; 50% increase in the separating force limits between CS coils; small change in turns for coil PF2; and a resizing and relocation of coil PF6 closer to the plasma. In addition the dome of the divertor, and the inboard slot design have been changed. The resulting improvement in the operating space in terms of flux consumption and plasma inductance is shown in fig 7(b). An important by-product of this optimisation is the availability of a substantial operating space for a reference H-mode discharge at 17 MA. The divertor modification (shown in fig 8), has been analysed [21] and it is found that the reduction of the dome makes the divertor more in-out symmetric, which is beneficial for the target peak-power loading but decreases the helium removal performance slightly. The new divertor also has a degree of detachment symmetry control by changing the position of the separatrix strike point at the inner target.

The vertical stability (VS) control for ITER has been modelled [22] and an ITPA multi-machine experimental collaboration has established the safe limits for a vertical stabilisation system's performance [23]. These studies have led to

recommendations for improvements to the ITER VS control. The experiments establish that for robust control against vertical displacements of the plasma, and taking into account the likely noise in a practical VS systems detection circuits, the stabilisation of a maximum vertical displacement (Δz_{max}) of at least 5% of the plasma minor radius is required (($\Delta z_{max}/a \geq 0.05$). For the ITER baseline VS system (dubbed 'VS1'), consisting of supplies to the PF coils PF2-PF5 (see fig 7(a)), the capability is only $\Delta z_{max}/a \sim 0.01$. The modelling and experiments suggest improvements will come from a combination of increasing the power supply voltage to the VS1 coils by 50% to 9kV, and connecting another circuit, VS2, consisting of two of the inner CS coils in parallel with a 6 kV driving voltage. This increases $\Delta z_{max}/a$ to ~ 0.023. The final improvement to 0.05 would come from a pair of in-vessel poloidal coils symmetrically placed about the median plane and situated behind the blanket modules. These coils have been amalgamated in a design to include ELM-mitigation, as detailed below.

The damage done by ELMs to the PFC material, and especially the divertor region, is a major concern for ITER. Previously presented multi-machine scaling studies [24] show that at low collisionality in the ITER range, an energy-loss per ELM (ΔW_{ELM} of ~ 20% of the energy stored in the pedestal (W_{ped}) can be expected. As the 15 MA reference discharge is predicted to have ~ 100MJ in the pedestal, values of up to 20 MJ can be expected if ELMs are not mitigated. Several aspects of the ELM damage and mitigation studies for ITER were presented: the physics specification for the ELM loads on PFC and divertor were summarised from present multi-machine studies [25]; the overall strategy for mitigating ELMs on ITER [26]; experimental measurements simulating ELM damage in a plasma-stream [27]; and the developments in 'ELM-pacing' by pellets [28]. The multi-machine studies show that the energy density in an unmitigated ELM can reach ~ 10 $MJ.m^{-2}$ at the target. This energy density, which is predicted from the multi-machine studies to reach the target in around 250 μs, is, on the timescale of an ELM event, many times that needed to evaporate any target material. The damage studies of CFC and tungsten targets show that ~ 0.5 $MJ.m^{-2}$ is around the limit to avoid melting of tungsten (see fig 9(a)), in line with the emerging database on effects in CFC and tungsten, summarised in fig 9(b). These data indicate that the transient heat load from ELMs needs to be reduced to a maximum around 0.5 $MJ.m^{-2}$, and for a lifetime of ~ 10^7 ELM events, considering the in-out ELM asymmetry [25], the ELMs must be limited to energies below 1 MJ [26]. Two methods are considered in [26], 'ELM-pacing', or stimulation of lower energy ELMs by disturbance of the plasma edge with injected deuterium pellets, and ergodisation of the plasma edge layer using Resonant Magnetic Perturbation (RMP) coils. Each of these methods has a growing database on existing machines. In order to reduce the period for growth of ELMs, the pellet pacing frequency for ITER will have to be in the region of 40 Hz, and pellets will need to penetrate to the top of the pedestal. To minimise the effects of accompanying convective energy loss at these high frequencies, development of a high speed pellet injector is required, and the first steps in this process are described in [28]. To accommodate pellet pacing the gas throughput requirements for ITER have been increased for the 400s standard burn 15 MA pulses by two-thirds to ~

200 $Pa.m^3.s^{-1}$.It is expected that the requirements for the pellet injector will be amended after further experiments on existing machines, particularly JET. The data from RMP experiments on existing machines, summarised in [26], have been used to guide the design of such a system for ITER. These experiments show it is possible to suppress ELMs at edge collisionalities relevant to ITER, whilst maintaining energy confinement times at values required by the ITER database ($H_{98y2} \sim 1$), provided the perturbations are sufficiently localised at the plasma edge. There are still many factors in the ELM stabilisation to determine, for instance the roles of edge-pumping and edge rotation in determining the penetration of the perturbation and the efficacy of the stabilisation. Nevertheless the experiments show that the coils should be as close as possible to the plasma edge, to maximise the edge perturbation and minimise the core perturbation. They should also be at the outboard side, but not only on the outboard mid-plane, and should provide a perturbation pitch-aligned as closely as possible to the unperturbed equilibrium. The width of the edge region having good overlap of magnetic islands from the RMP coils' vacuum field should also exceed a threshold value, given by the so-called Chirikov parameter. Using these design guides, and the constraints of the ITER vacuum vessel fabricability, the only feasible RMP coil design emerged as shown in fig 10, where the coils are combined with those indicated as required for vertical stabilisation [22]. The required coil currents have been evaluated previously [30] in the range of several 10s of kA, and 60 kA peak is chosen for these coils, values which are in line with the VS requirements. The mid-plane coils are mainly used to trim the perturbation to reduce magnetic braking effects, and avoid locked modes, whilst the coils above and below mid-plane provide most of the resonant contribution.

The RMP ELM coils have the added benefit of the ability to enhance the stabilisation of Resistive Wall Modes (RWM) in ITER, as summarised in [17]. Use of all three rows of coils allows RWM stabilisation up to $\beta_N = 3.74$, whilst use of the top and bottom coils only take this figure to 3.83.

Disruptions are a major concern in ITER, as it will have by far the highest stored energy of any fusion device to date, and thus there will be the biggest potential impact from thermal energy loss to the plasma facing material surfaces or halo current forces on the vessel structures. In addition, the large plasma current gives the potential for MW-levels of Runaway Electron (RE) beams to be generated in the high electric fields caused in a disruption. These beams would impinge on very localised areas and lead to severe melting damage to first wall components. To mitigate the effects of disruptions, Massive Gas Injection (MGI) systems have been defined [31], and initial hardware examples tested [28]. The amounts of gas delivered by an MGI system must be large (in the 10-several x100 kPa. m^3 range), and must be delivered on a timescale of a few ms, determined by the rapid avalanche growth rate for RE populations in ITER conditions. The amounts of impurity gas required to cool the plasma radiatively (thus reducing the thermal loss in PFCs) and raise the resistivity (increasing decay times and thus reducing halo current forces) are ~ 20 $kPa.m^3$ for 100% neon gas introduction. The amounts to

quench the growth of RE populations can be much higher, as a specific density limit (the Connor-Hastie-Rosenbluth, or CHR limit) must be exceeded for collisional suppression of the Dreicer –field electron acceleration. In ITER this CHR density is ~ 5 10^{21} m^{-3}, and is around 5-10 times higher than the density at which the thermal and halo current effects are suppressed. The quantities to exceed the CHR limit have been evaluated [30] on the basis of extrapolation from present experiments and using a 0-D radiation balance model. The two methods agree well for the high-Z gases like neon, but the latter method tends to give much higher quantities for the low Z gases. The authors of [31] estimate that ~ 26 kPa.m^3 of neon would be required to exceed the CHR limit, but this rises to ~ 500 kPa. m^3 for hydrogenic species. This quantity of hydrogen injected into the ITER vessel would exceed the deflagration limit for the cryopumps. A similar quantity of Helium would certainly cause the in-vessel cryopumps to regenerate and lead to loss of vacuum conditioning, but the authors nevertheless recommend that the capability to inject such large quantities, with a rise time of ~ 3 ms, be maintained, as the light gases have a much higher sound speed, enabling the quick delivery, alongside the preferred option of neon, which does not have any serious vacuum side-effects. The progress in realising the necessary delivery systems at ORNL [28] has produced single and multi-headed fast gas valves capable of delivering 3 10^5 – 10^6 Pa. m^3s^{-1} of deuterium with an exit pressure of > 3 MPa, and a rise time of ~ 1ms. These will be tested on the DIIID tokamak in 2009. In addition, a concept pellet pipe gun has been produced, which will produce cryogenic pellets for injection against an angled plate target, the shattered pellet fragments being directed towards the plasma, where it they should form an injected mass which will be assimilated into the plasma core more efficiently than a gas plume. The pellet gun concept (shown in fig 11), will be optimised for minimum plume angular divergence and tested on DIIID in 2009.

The first wall of ITER has been undergoing re-evaluation [32], based on the new predictions from the ITER physics database [24], extended at this conference [25]. In the previous design, misalignment steps of 2mm between modules were considered, and the parallel heat flux deep into the Scrape-off-layer (SOL) was assumed to be small. Now a 5 mm step misalignment is considered more achievable, and the evidence [24], [25] points to fast radial transport deep into the SOL, giving high parallel heat fluxes. To a certain extent the new start-up and ramp-down scenarios, featuring early and late transitions to X-point [18], [25], limit the heat flux to the wall, but, depending on the number of limiters, parallel flux at the plasma limiter surfaces can be in the range 30-80 MW.m^{-2}, the lower value being for 9 limiters at inboard or outboard, which are now replacing the original design with only 2 . The predicted parallel power fluxes in steady state (inter-ELM) to the inner and outer walls are up to 5 MW.m^{-2} and 3 MW.m^{-2} respectively. At these levels the continuous loading will represent a challenge to the integrity of the edges of first wall tiles such as those constructed by the Chinese ITER partner, results from which were presented at the conference [33]. These components are fabricated by hot-isostatic pressing (HIP) of a beryllium PFC layer onto a CuCrZr heat sink and a stainless steel back plate. A mock-up was tested through 500 cycles at 1.47 MW.m^{-2} and a couple of cycles at 2.47 MW.m^{-2}, without visible damage, but with

clear NDT-detected cracking at the Be-CuCrZr inter-metallic layer. Such technologies need further development before sufficient safety margin is achieved to withstand the fatigue cycling which could occur in ELMs. The estimates in the new physics simulations show time-averaged parallel loads during an ELM at the level of 5MW.m^{-2} for the inner and outer walls, and up to 25 MW.m^{-2} at the top X-point. To cope in the latter region, even with a shallow incident angle, the design may be forced to adopt technologies outside the present design, such as hypervapotron elements [32].

3.2 *Superconducting Magnets*

Since the 21st IAEA FEC in 2006, there has been significant progress on all aspects of the ITER superconducting magnet system, and this was summarised in a contribution by Weng et al [34]. The cyclic degradation phenomenon on the TF superconductor samples, which had caused so much concern has been revisited; the PF conductors specification has been redefined following the results of the 15 MA scenario optimisation, and the NbTi coil characterised; a high accuracy automatic coil winding head has been developed and tested; radiation-resistant Cyanate Ester epoxy development has proceeded; and the production of High Temperature Superconductor (HTS) 68kA current leads for the TF coils has proceeded ready for testing in the Chinese Domestic Agency programme.

Following concerns about the degradation of the current-sharing temperature (T_{CS}) in the ITER TF Nb_3Sn conductors seen in 2005-6, a major R&D programme was launched to identify and solve the problem. The programme involved testing at the PSU/CRPP SULTAN facility at Villigen in Switzerland, for degradation in T_{CS} over 1000 strain cycles at current of 68kA in an 11.8T field, representing the upper end of the ITER requirements. During the tests it was established that the previous results had been sensitive to the joint current in the samples, and the degradation had been incorrectly assessed. The SULTAN sample instrumentation was also improved to achieve better alignment between calorimetric and electrical measurements of T_{CS} [35]. A major step-forward in improvement of the conductors themselves has been the realisation that long-twist pitches can improve conductor performance. The cabling design has therefore been redesigned to include long-twist pitch in the inner cabling stages. By the time of the conference, 9 prototype TF samples (with 18 different conductor legs) had been tested. The target performance was to maintain $T_{CS} > 5.7$K (outside the errors) after 1000 cycles, with no change in value (<0.1K) over the last 400 cycles. The results for the tested samples are shown in fig 12. Sufficient 'good samples' with T_{CS} above 6K (target plus headroom) have now been measured to give confidence that the TF strands perform adequately in the reference configuration (the poor performance of the two legs of sample 6 has been identified as due to an obvious error in preparation).

Following the re-evaluation of the 15 MA scenario as discussed in section 3.1, the parameters of the PF coils were redefined as in table 1(a) and (b). The new specifications indicate the requirement for performance above 50 kA in several

coils. The main changes to the PF conductors for the low field (PF2-PF5) coils can be seen from table 1(b) to be a decrease in the Cu: non Cu ratio, increasing the superconductor area and ensuring sufficient temperature margin. At the same time the AC losses in the pulsed operation must be minimised to limit the temperature increase. In addition, the PF6 magnetic field requirements are on the edge of the capabilities of NbTi and require sub-cooling. Previously, short sample tests of the PFI NbTi conductor, similar to that in PF1-PF6, had shown that above a threshold current level of 30-40 kA, the quench current was well below the expected strand critical current. With the changes to the conductor, and the new extended requirements it was essential to test a long length of the PF conductor. This has been achieved with the test of the Poloidal Field Conductor Insert (PFCI) coil at the CSMC facility in Naka, Japan [36]. The PFCI is a single turn coil (see fig 13(a)) with a long length of conductor similar to that used in PF1 and PF6, with a similar joint technology. Fig 13(b) shows the installation of the coil at CSMC. The tests included AC and DC behaviour and showed that, unlike the short sample tests, the performance of the quench point of the conductor (in terms of critical field, current, or temperature) is very close to the sum of the measurements made on individual conductor strands. An example is shown in fig 14, where the difference between the critical current at quench in the conductor at a particular peak magnetic field ($I_C(B_p)$) and the sum expected from the sum of the strands evaluated at the same peak field (I_c^{strand} x no of strands) is plotted for short samples and PFCI. The PFCI is seen to out-perform the short sample tests, giving a much closer performance to that expected from the strands. In general the performance of the PF insert coil was excellent, exceeding that of the short samples by up to 0.5K, and much better than that required to meet the PF coil performance requirements. Test results give confidence that the PF conductor will exceed design target performance, and suggest that sub-cooling may not be required.

In terms of TF coil fabrication, key components of the TF-coil radial plates manufacturing have been developed with Japanese industry [34, 37], and the Japanese Domestic Agency has developed a high accuracy automatic winding head (see fig 15) and performed a trial winding. The accuracy obtained is ±0.035% in radial position, which corresponds to ±0.85mm and ±1.85mm at the inner and outer equatorial positions respectively, and ±2.35mm at the coil top and bottom.

It is well-known that epoxy resin is at the limits of its radiation resistance at the ITER fluence levels of 10 MGy (10^{22} neutrons per m^2). Cyanate Ester (CE) resins have a higher radiation resistance, but a higher cost and a less well-established manufacturing base. The European Domestic Agency has developed with industry a blended CE (60% CE: 40% epoxy) and this achieves the requisite strength retention at 20 MGy – double the ITER design requirement. Large scale industrial fabrication trials [38] have shown that the rate of the strongly-exothermic curing reaction of the resin mix can be controlled and that it has a long enough pot life to impregnate the large TF coils.

3.3 *Diagnostics*

The recommendations of the ITER Diagnostic Working Group (DWG) in the ITER Design Review were reported [39], along with the current main R&D needs for diagnostics [40]. The DWG made recommendations for omitting some diagnostics, principally the Divertor Reflectometer, Electron Cyclotron Absorption measurement, Visible Continuum Array and Water Neutron Activation system. It also recommended installation of only the front end of some diagnostics, leaving extension to a second phase. Finally, it recommended additions to the basic set, including a high resolution neutron spectrometer, neutron calibration in the divertor, infra-red thermography, Collective Thomson Scattering and Dust and Tritium measurement to support the licensing of ITER.

The most urgent of these diagnostic recommendations relate to the measurements of in-vessel dust and tritium inventories. As discussed in the paper on ITER licensing [16], the Safety Case for ITER operation will put limits on these inventories. For dust, where the issues are radioactive content, toxicity, tritium retention, possible hydrogen production with steam from an in-vessel leak and explosion in air, the in-vessel limit will be < 1 tonne, with ≤670 kg being the practical limit to allow for uncertainties of measurement. For tritium, where the issues are radioactive content, toxicity and possible explosion/flammable reaction with an in-vessel air leak, the corresponding limits will be ≤ 1 kg, with ≤700g being applied to allow for measurement uncertainties.

The systems proposed for the dust and tritium measurements include a divertor erosion monitor, dust microbalance, laser desorption to get a local concentration of tritium during shutdowns and removable samples. An electrostatic dust detector has been developed [41]. The detectors have a very fine grid, making it possible to detect particles in the 1-2 μm range. The conductive grids also evaporate the dust particles landing on the conducting strips. Miniature sparks occur when dust particles land on the conducting strips and the voltage pulses are counted by nuclear counting electronics. Particles of different sizes (in terms of μg/unit area) are seen to give different size current pulses, the larger the particle, the longer the pulse. Eventually all particles are vaporised by the detector. The device works well in either atmospheric or vacuum conditions, and the response of the detector to particle size is shown in fig 16. Work is in progress to ruggedise the front end circuit board and wire array, and develop its use with refractory metals. Another diagnostic being developed for dust measurements comes from work by the TEXTOR team [40], and involves a multi-purpose Nd:YAG laser-based system that combines laser-induced breakdown (LIB), ablation and desorption spectroscopy with Mie/Rayleigh scattering and quartz microbalances for measuring tritium retention, desorption and dust. An overview of this is shown in fig 17.

In addition to the dust diagnostics, the International Tokamak Physics Activity (ITPA) Topical Group (TG) on diagnostics has identified three more ‘high priority’ topics for focus of current R&D. These are: development of methods of measuring

the energy and density distribution of confined and escaping α–particles; assessment of the options for the vertical neutron camera to measure the 2-d n/α source profile and its asymmetries; and the development of first mirrors that can survive the ITER environment. The first two were covered in the review paper [40], whilst the third was the subject of special presentations [42],[43] and [44], the last of which also dealt with in-situ calibration. The TEXTOR group find that deuterium gas flow across a mirror surface is effective in avoiding carbonaceous build-up [42]. The Russian group have also experimented with 'gas blowoff' techniques but also laser cleaning (including tests in Tore Supra), plasma discharge cleaning and high temperatures, all of which have some success [43]. In addition, coatings such as Ta_2O_5 and Al_2O_3 are found to delay the need for cleaning. The survivability of first collection optics is a key point for the ITER Divertor LIDAR [45], and the progress in optical component protection and cleansing was highlighted. Modelling has given a guide to the expected mirror surface damage in ITER locations. The first modelling of the first mirror position of the ITER MSE diagnostic has resulted (table 2) in figures which show that the sputtering of tungsten will not cause a problem in this position. The attenuation for beryllium is also fairly good, but because the SOL in ITER may contain a significant fraction of beryllium from the first wall, the behaviour of sputtered beryllium layers is the subject of much evaluation, it being found that Be layers may exhibit high levels of porosity which makes their reflectivity much lower than pure Be [47]. Further modelling [42] using the full atomic package of EIRENE, realistic edge conditions and the full charge states of the hydrogenic ions, helium, carbon and beryllium shows the complex situation for first collection optics as a function of position, with the upper port core-CXRS mirrors being under net erosion conditions for carbon, whilst the midplane core-LIDAR mirror [45] is under net deposition. The situation for beryllium on the other hand, shows erosion and deposition almost in balance. Defining cleaning strategies will clearly be an extremely complex task.

3.4 *Heating and Current Drive and Fuelling systems*.

The majority of the progress on Heating and Current Drive (H&CD) systems described at the conference referred to activities related to ITER, although not all papers submitted were in the IT category, but some were selected under FT. Both sets are discussed in this section.

Whilst on present tokamak devices the majority of the plasma heating data, and almost the entire dataset on high performance plasmas, is provided by Neutral Beam Injection (NBI), the H&CD system which is nearest to reaching its ITER parameters is the Electron Cyclotron Resonance Heating (ECRH) system [48],[49]. This is due to the performance of the 170 GHz gyrotron sources, and in particular of the Japanese ITER gyrotron prototype, fig 18(a), (b). This gyrotron features a triode gun and has a control anode enabling beam voltage and pitch factor to be controlled independently, which enlarges the operational region. It has achieved 1 MW output for 800s at 55% efficiency, exceeding the ITER specification of 1 MW/500s/50%.

It has also operated for 0.8 MW pulses of 400s length every 30 minutes, in a simulation of the ITER pulsing conditions. The Russian gyrotron prototype for ITER, with a diode gun, has achieved 1MW for 112s at 53% efficiency, and has now moved to a new test stand at Kurchatov, as the old test stand was limiting performance [50]. The EU development of gyrotrons for ITER is now focussing on a 2MW coaxial cavity gyrotron [51]. This is so far limited to 1.4MW output for a few ms. Whilst parasitic low frequency oscillations have been significantly reduced, at the higher voltages near the nominal parameters, parasitic high frequency oscillations (f~ 160 GHz) appear simultaneously with the target gyrotron working mode. These are thought to be excited in the beam tunnel, and investigations to suppress them are ongoing. Outside of the ITER programme, the difficulties of producing series gyrotrons all of which reach the target parameters are now being seen in the 140 GHz gyrotrons for W-7X [52]. Whilst one of the three series gyrotrons reached close to the target 1 MW level for 30 minutes (0.92MW at an efficiency of 43% was achieved), the other two failed because for high output power there was deterioration of the vacuum pressure in the tube. Measurements show the existence of several frequencies in the range 119 – 132 GHz excited alongside the main mode at 140 GHz. The source of these problems is still under investigation. In spite of these adverse results in the gyrotron programme, it now seems timely to test the plasma performance of a pure ECR – heated plasma in a large tokamak at high power (> 10 MW). The prospects for the more forensic use of EC waves on ITER, the stabilisation of Neoclassical Tearing Modes by Electron Cyclotron Current Drive (ECCD) look generally favourable from present data and simulations of the modified Rutherford Equation (MRE) describing NTM island growth [53]

Unlike the ECRH midplane- [54], and upper-port launchers [55], which have not changed significantly since the 2006 FEC, there has been the selection of an ICRH antenna design following the ITER design Working Group deliberations in 2007. The new design, from the EU laboratories, was presented at this conference [56]. The design is shown in section in fig 19. It comprises a port plug housing four RF power modules, each of which mounts six straps collected in triplets to eight feeding transmission lines. Protection for the modules is provided by a series of Faraday screen bars. The rear section of each transmission line forms a Removable Vacuum Transmission Line to enable RF windows and key diagnostics to be replaceable from the port plug rear, without removal of the entire plug, in case of damage. Most of the interior of the modules contains shielding material to reduce neutron flux and consequent activation at the rear of the module. The design includes RF diagnostics for matching the system and providing the measurements for arc detection. The proposed matching system for the antenna, using a conjugate-T network, was also presented [57]. The ITER antenna uses a close-packed ‘resonant double –loop’ strap array to enable the achievement of high power density coupled to the plasma (8-10 $MW.m^{-2}$ for a 20 MW antenna). The conjugate-T matching is intended to achieve ELM-tolerance, ie. avoid the tripping of the RF power to the plasma due to reflected power transients occurring during the edge plasma changes accompanying an ELM which lead to a change in the ‘coupling

resistance' of the plasma as seen by the antenna. Two key tests of this concept on tokamak plasmas are now nearing completion and were presented. On Tore Supra [58], an ITER-like antenna with conjugate-T has been tested on plasma with ELMs simulated by supersonic molecular beam injection (SMBI), whilst on JET, a larger ITER-like antenna has been successfully installed and has coupled power into L-mode and ELMy H-mode JET plasmas [59]. The two antennae are shown in fig 20 (a) and (b) respectively. Their performance under simulated or real ELM conditions is encouraging, with the Tore Supra ILP (fig 21(a)) and the JET ILA (fig 21(b)) continuing to couple power to the plasma during the ELM-simulated and real-ELM events respectively. Commissioning of the JET ILA to full power continues, with the status reported at the conference being 1.8 MW maximum (from half an antenna) in the H-mode (corresponds to ~ 3.8 $MW.m^{-2}$) and 3.8 MW maximum from the full antenna (5.8 $MW.m^{-2}$) into the L-mode. Initial modelling with the TOPICA code shows that the edge coupling conditions in JET extrapolate to ITER such that the 20 MW from the ITER ICRF module [56] looks achievable, given the assumptions about the edge plasma, which are of course, crucial. There remains the serious issue of the effect of the RF sheath on the generation of impurities, especially in machines with tungsten or other refractory metals. This was covered in presentations in the EX sections of the conference [60 – 62].

Since the 2006 FEC meeting, important scheme design choices have been made for the ITER Negative ion Neutral Beam Injection (NNBI) system. The RF-excited Negative Ion source, as developed in the EU, has been chosen for the plasma source, and the Multi-Aperture Multi-Gap (MAMuG) design, as developed in the Japanese programme, has been chosen for the accelerator. Progress on the RF source [63] has established up to one-hour long stable pulses with >200 $A.m^{-2}$ negative ion current density in deuterium (D^-). This satisfies the ITER target, but must be extrapolated to a full-size source. Covering the source's copper walls with molybdenum has avoided copper self-sputtering which otherwise deteriorates the sources cesiated surfaces, reducing negative ion yield. With molybdenum cover it is easier to achieve a ratio of extracted electrons/negative ions below unity (the ITER target), as shown in fig 22. The tests on the different ITER accelerator concepts (MAMuG and the EU SINGAP) showed [64] that the MAMuG achieved superior voltage holding, and a much lower co-extracted electron power. The latter comparison indicated an order of magnitude lower extracted power when extrapolated to full-size accelerator (800 kW for MAMuG against 7.3MW for SINGAP). Both the unacceptable power drain for the SINGAP case, and the problem of designing dumps to handle the extracted electron power, led to the adoption of MAMuG. Nevertheless, the progress towards the achievement of holding 1 MV (the ITER NNBI target) on the MAMuG accelerator remains slow, with 796 kV being the limit reached on a few aperture system at a current density of 140 $A.m^{-2}$. Other papers on the NNBI system described the progress in the Japanese design of the 1 MV extraction power supply design [65] and the cryopump design for the NNBI beamlines, as developed at Fz Karlsruhe [66]. The NNBI system for ITER has a key role in driving non-inductive current in the plasma, to aid the achievement of long-pulse conditions. The experimental evidence on NBI current drive on present machines has thrown up

some questions regarding the off-axis efficiency, but as different code predictions are used to compare with experiment, a comparison of the codes themselves in ITER conditions is required. One such comparison, between three orbit-following Monte Carlo codes and two Fokker-Planck (FP) -based codes was reported [67]. Although there is agreement on the initial fast NB ion source and the heating source profiles from the Monte Carlo codes generally agree, there are differences in the details of energy partition to electrons and ions. The FP codes predict different fast ion currents at >40% of the minor radius of the plasma, pointing up the problem of comparing experiment to a particular code. Reference [67] discusses the origins of discrepancies.

A potential Lower Hybrid system for ITER, featuring a Passive-Active Multijunction (PAM) device, has been the subject of an EU design effort and was reported [68].

The activity on study of fuelling systems continues to be an under-represented 'Cinderella' subject, with only one contribution on pellets [28] in the ITER section and one in the FT class [69]. The development of pellets at ORNL for fuelling, as well as ELM-pacing and disruption mitigation (as described in section 3.1 above) was reported. The ITER pellet fuelling requires 100 $Pa.m^3.s^{-1}$, which requires production of 1.5 $cm^3.s^{-1}$ of solid ice, five times higher throughput than previously achieved with a continuous extruder. A novel twin-screw approach is under development and test and promises greater throughput and stability than a single screw, avoiding for example the friction drive heating of a single screw. Models to predict how pellets will fuel ITER [70], [71] show that most ablation is expected in the pedestal region ($0.95 > r/a > 0.85$), but that for injection from the high-field side of the plasma, the grad-B drift pushes the neutral cloud of the pellet to deposit in the inner region ($0.65 > r/a > 0.4$). The problems of high-field launch are related to the tight bends required of the pellet-guide tube, which cause centrifugal forces on the pellet and lead to pellet disintegration above ~ 300 $m.s^{-1}$ velocity. At these maximum velocities the pellets will not penetrate the high-field side pedestal without ablation. The authors of [69] propose using techniques from the fabrication of Inertial Confinement Fusion (ICF) pellets to create polymer or foam shells (deuterium/carbon based only) for the deuterium-tritium ice. These are predicted to have between 25 and 100 times the yield stress of the pure D-T ice at cryogenic (6K temperatures), perhaps giving a 5-10 times higher injection velocity capability. Also proposed is the development of pellet acceleration systems using ablation of material following absorption of microwaves from gyrotrons in metallic dust micro-particles in the pellet fuel. Tests using zinc dust in paraffin, to establish the potential for energy absorption, are in progress

4 Divertor Technology and Plasma Facing Components and Materials

4.1 Divertor Technology

Two novel divertor technologies were represented at the conference in the FT sessions: the helium-cooled tungsten divertor design; and a liquid lithium divertor design.

The helium-cooled divertor design developed at Fz Karlsruhe [72] is a so-called helium multi-jet (HEMJ) concept and features reduced activation steel thimbles with a small tungsten tile cap. The thimbles are cooled by helium internal jets, and are assembled onto modules and then into the full divertor, as shown in fig 23(a). The helium coolant is at 600ºC, and the tile design should keep the surface temperature below the 1300ºC limit, inside the window for tungsten re-crystallisation . The 600ºC limit is a lower temperature limt coming from the necessity to remain above the ductile-brittle transition temperature for tungsten. The joining to the steel is achieved variously by an intermediate tungsten alloy cap, and intermediate W/W-alloy/steel brazes with braze temperature of 1050ºC, or a braze direct to the steel. The HEMJ fingers have been tested in an electron beam and shown to be capable of handling 10 $MW.m^{-2}$ power loading. Repeated cycling tests are now in progress, and individual designs have withstood up to 200 cycles at 10 $MW.m^{-2}$ without damage (example shown in fig 23(b)). The full design of this divertor is complex and would contain ~ $2 .10^5$ individual thimbles for a reactor.

Several tokamaks have reported improved performance with lithium surface coating. The progress on liquid lithium divertors as developed at the Russian programme was reported [73]. The concept uses the lithium-filled Capillary Porous System (CPS), with plasma-induced melting and evaporation of lithium held in a higher melting point metal matrix. After prototype tests on the SPRUT-4 linear plasma device and electron beam power loading tests up to 50 $MW.m^{-2}$ (held for 5 s), CPS devices have been tested on tokamaks T-10, T-11M and FTU. There are now design proposals for CPS-based divertors for T-15 and KTM [9], and also a single-element continuously cooled lithium limiter for the FTU at Frascati. The proposal is shown in fig 24, and features a lithium-filled CPS in a tungsten fibre matrix.

4.2 *Plasma Facing Components and Materials*

Several contributions addressed plasma-wall interactions and tritium-retention issues in tokamaks with metal walls. The key plasma surface interaction issues of an all-metal PFC system in ITER were assessed for the tungsten divertor and beryllium or tungsten first wall case, and conclusions drawn for DEMO [74]. The authors studied sputtering, transport, formation of mixed surface layers, tritium co-deposition, core plasma contamination, ELM-response and helium-irradiation effects on tungsten. Apart from various analysis packages, data from PISCES were used to assess PFC performance. Erosion prediction results for the ITER outer first wall under load from the Q=10 baseline plasma with a reference case ‘convective’ plasma edge regime are shown in table 3. The convective regime results in a 50-fold

increase in flux to the walls over a case with diffusive transport only. A comparison of beryllium and tungsten and a reference bare steel wall is made. The predicted erosion rates (0.3 $nm.s^{-1}$ for Be and 0.002 $nm.s^{-1}$ for W) are acceptable at ITER's low duty cycle, but for a reactor, only tungsten extrapolates to acceptable levels. Most sputtered beryllium is predicted to be re-deposited on the walls, but about 10% gets to the divertor dome. Tritium co-deposition with beryllium could be as high as 1.5 - 1.8g per full-power 400s shot, making operation marginal. The presently envisioned 300ºC wall temperature for ITER will drive out 50% of the co-deposited tritium, but this could be increased to 85-90% by installing a 400ºC wall-baking capability[75]. Tritium retention in tungsten is found to be negligible. The retention of tritium on carbon is assessed as ~ 3g per full-power shot, taking a carbon vessel to the practical 700g inventory limit [16] in only ~ 230 shots. On the other hand, Roth [76] estimated 800-900 DT shots before the limit is reached, in an IT-session contribution. There is clearly still a need to examine the assumptions in these complex modelling exercises. The simulations in [74] show that Be, bare steel or even W contamination of the plasma from sputtering should not cause unacceptable levels, the situation with tungsten arising from the ionisation of sputtered tungsten ions very close to the wall (~4 cm), and their loss in the scrape-off layer. This result, in spite of the differences in plasma conditions, is not necessarily easy to reconcile with the problems of impurity accumulation seen with tungsten walls in ASDEX-Upgrade [77], [78]. The possible formation of Be-W inter-metallics by re-deposition of Be on tungsten divertor surfaces is thought to be unlikely in ITER, as the process only accelerates above ~ 750ºC [74, 79], and the divertor strike zones are predicted to stay below 800ºC, not enough margin to overcome the natural barrier to Be-W formation which would come from re-sputtering of Be from the divertor. The simulations and tests of ELMs on the tungsten surface give predicted safe (no melting) ELM values for tungsten as shown in fig 25. Given the predicted rise times for ELMs on ITER in the 0.2 – 0.5 ms range [24], the safe ELM limit is similar to the 0.5 $MJ.m^{-2}$ limit already discussed in section 3.1 above. Finally ref [74] discusses the situation regarding helium effects on tungsten. Tungsten 'fuzz', tendril growth on the surface due to He-ion bombardment, is only seen as a problem at high temperatures (beyond 700ºC), whilst helium blistering due to nano-structure formation at lower temperatures is seen, from results in the Large Helical Device [80] with pure He plasma, to be acceptable at a predicted < 0.6 $nm.s^{-1}$ in the divertor for a <10% helium concentration.

Experimental studies of deuterium retention in tungsten and molybdenum, were reported [81], the deuterium being a proxy for tritium. The data were taken in the Pilot-PSI linear device, which can irradiate surfaces with plasma streams of electron density $\leq 10^{21}$ m^{-3} and electron temperature ≤ 5 eV, simulating the ITER edge. The measured retention of deuterium in tungsten was very low ($D^{retained}/D_{incident} \sim 10^{-7} – 10^{-5}$), which is encouraging for reactor conditions. There seems to be no measurable dependence on deuterium fluence, as shown in fig 26. The retention in molybdenum is significantly higher (by over a factor 10), at low fluence, but the results come together at higher fluence. This may be due to the co-deposition of

boron and carbon in the tests, due to the sample preparation, a fact realised only in the results stage, where boron and carbon were seen on the molybdenum surface. As the presence of boron and carbon in current tokamaks is often the case, tokamak results citing problems of retention with molybdenum (eg. Alcator C-MOD), may be a side result of this. Further tests with cleaner molybdenum surfaces are planned at Pilot-PSI.

Glow discharge cleaning (GDC) is a well-established technique to clean and restore the surface of tokamaks after opening for maintenance or unscheduled leaks or disruptions. It cannot be applied in a magnetic field and is hence of no use for the tokamaks with superconducting toroidal field coils, such as ITER, where the TF should remain on to avoid cryostat warm-up and loss of operational time after a disruption or minor leak. An alternative of conditioning with ICRF power (Ion Cyclotron Wall Conditioning –ICWC) has been developed on TEXTOR and other devices, and was presented [82]. For standard wall conditioning, a mixture of H_2/He is recommended, whilst for removing tritium O_2 with He provides the most effective scenario. N_2-H_2 or N_2-D_2 mixtures were ineffective in TEXTOR conditions because of strong absorption of nitrogen in the wall. Although the discharge cleaning results show toroidal symmetry there are poloidal asymmetries. These have been improved by employing mode conversion techniques in RF plasmas with two ion species in tandem with a small vertical field, but much more work is needed here.

A key factor for the production of PFCs for ITER, and even more so for the reactors to follow it, will be the quality control of the multiple units and the need for non-destructive examination techniques to prove unit integrity. Two presentations at the conference addressed this issue. The Japanese ITER domestic agency has developed the Far Infrared Non-destructive examination of Divertor (FIND) test system using infrared examination of the surface of an element through which alternate hot and cold water flows [83]. The test has the ability to spot flaws in the joints in the element. In the EU programme, the SATIR infrared NDE test method also uses the infrared detection of delays in surface temperature change when fast flowing water in an element is changed from hot to cold. It has been applied to the European Vertical Target Qualification Prototypes [84]

5 Fusion Materials and Blanket Research

In the context of this review, ‘Fusion’ materials are those used in the structure of the vessel and internal components in a fusion device and those used to fabricate a breeding blanket, for either their structural or nucleonics properties, the plasma facing materials having been covered in section 4.

An overview of the work being carried out in Japan under the Japanese-EU ‘Broader Approach’ was given covering both materials and blanket concepts [85]. The more detailed papers supporting this are also discussed below.

5.1 *Fusion Materials*

The work on Reduced Activation Ferritic-Martensitic (RAFM) steels continues to make progress. In large-scale production of RAFM steel, impurity removal is important because large quantities of scrap steel will have to be used. The Electro-Slag Remelting (ESR) of the Japanese RAFM steel F82-H was reported [85]. All the Tantalum containing oxides were found to be removed in the ESR process. Progress has also been made in the joining of the EU Eurofer RAFM steel, in establishing the heat treatment of welds in Eurofer. Heat treatment in the range 700º (electron-beam welding) to 740ºC (TIG welding) gives a Ductile-Brittle Transition Temperature (DBTT) closest to the base material [85].

The impact of neutron damage on Eurofer and F82-H has been studied at temperatures up to 350ºC and doses up to ~ 70 dpa in in-pile irradiation experiments [86]. The change in the DBTT (ΔDBTT) is found to reduce as the temperature at which the irradiation is performed goes towards 350ºC, being significantly delayed to higher doses. Asymptotically the ΔDBTT is ~ 230ºC at 70 dpa and 300ºC - 350ºC irradiation, but for lower doses (~20 dpa) the embrittlement at 350ºC is much reduced (ΔDBTT ~ 70ºC) against the value of ΔDBTT ~ 180ºC for 300-330ºC irradiation. Such a low deterioration would allow the material to remain useful for a time-period similar to the interval between maintenance in a reactor (~ 1 year), but the problem of embrittlement during the cooldown and outage would need to be faced . However, it is shown that the annealing of the Eurofer at 550ºC post-irradiation enables the DBTT to be largely recovered to a low value well below room temperature (fig 27), and the residual hardening drops to a low value of ~ 24 MPa, (compared to several hundred MPa hardening post-irradiation) whilst the ultimate tensile strength almost completely recovers. This suggests a strategy for using Eurofer if a bakeout of the entire vessel structure were to be included in the reactor design. The results presented for F82-H steel in the Japanese programme also show a DBTT change of similar value to Eurofer, plateauing out above ~ 30 dpa [87]. Again the radiation hardening is improved by operating above 400ºC. The effect of irradiation on fatigue cycles is seen to be rather small.

The effect of helium production on embrittlement of the RAFM steels has been studied in fission-neutron irradiation of steels doped with boron [87], [88] and ^{58}Ni [87], to simulate the production of helium by the higher energy fusion spectrum. Ref [87] also featured some comparison with helium results obtained by dual-beam irradiation featuring Fe^{3+} and He^{+} beams. The DBTT shift in the Japanese B- and Ni-doped tests [87] were accompanied by varying degrees of hardening. These effects are difficult to separate out from the known effects of Ni-doping and B-doping on irradiation hardening. The effects of He production were not clearly identified below 400 appm He. The ion beam results produced a more clear-cut result that hardening is definitely seen to occur at He levels > 1000 appm and He-implantation rates of 100-1000 appm He/dpa, as shown in fig 28. The Eurofer studies [88] included boron doping of Eurofer with identical amounts (82 ppm) of

natural boron (^{nat}B) and ^{10}B. The enhanced post-irradiation He production with the pure boron isotopic alloy (415 appm against 80 appm with the ^{nat}B alloy) led to this alloy ("alloy 2" in the study) having consistently higher post-irradiation yield strength at all higher temperatures. Microstructure examination showed that the size of helium bubbles in the alloy increased with temperature, and the bubble-induced cavities were larger in alloy 2. Micrographs of fracture specimens of the alloys show clear 'fish-eyes' of local He-induced features (fig 29).

Oxide-Dispersion-Strengthened (ODS) RAFM steels are promising materials for fusion power structural applications at temperatures up to 750°C. They are produced by powder-metallurgy techniques, ie.by mechanical alloying followed by Hot Isostatic Pressing (HIPing) or hot extrusion. The comparative properties of ODS RAFM produced by various processes were presented [89]. The main findings are: planetary ball-milling is preferred to high-energy ball milling; hydrogen should be used as a mechanical alloying atmosphere (fig 30); a high degassing temperature $\geq$ 925K – should be applied to mechanically-alloyed powders; chromium content of ~ 14% yields better results than 12% (higher tensile strength and better Charpy-impact); and titanium oxide contents as high as 0.5% should be avoided due to embrittlement. The main problem with ODS RAFM remains the uncomfortably high value of the DBTT before irradiation, which is ~ 20°C even with the hydrogen alloying atmosphere (see fig 30).

SiC/SiC composites are promising candidates for advanced high temperature fusion reactor blanket design, as they offer inherently good chemical stability at high temperatures and low-activation and low after-heat properties. Research has now entered the databasing phase to establish the specific strength and strength retention of samples from the various fabrication methods. The properties of SiC/SiC produced by the nano-infiltration transient eutectic (NITE) method, developed by the Institute of Energy Science and Technology CO Ltd in Japan, were presented [90]. This work is carried out within the Broader Approach activity [85]. Samples of NITE SiC/SiC (see fig 31) were compared to samples from other fabrication methods such as polymer-impregnation-pyrolysis (PIP) and chemical-vapour-infiltration (CVI). It has been found that the energy release rate in cracks in NITE SiC/SiC is much lower that in PIP composites, leading to more crack resistance as this energy release controls crack density during the damage process. On the other hand, PIP SiC/SiC composites are more damage-tolerant. NITE-derived SiC/SiC is also more crack-resistant than CVI-derived composite. In cyclic loading-unloading tests the CVI material shows rapid modulus decrease on crack initiation, implying progressive damage accumulation. This improved crack resistance for NITE composite material gives a much better Helium gas-tightness (10^{-10} – 10^{-9} $m^2.s^{-1}$) compared to CVI SiC/SiC (10^{-6} – 10^{-4} $m^2.s^{-1}$).

Also in the framework of the Broader Approach activities, static tests have been carried out with SiC/SiC material and Pb-17Li eutectic, as foreseen in some liquid metal blanket designs [85]. These tests show, encouragingly, that the SiC material

had not reacted with the Lithium Lead.

5.2 *Blanket Research*

Many papers were presented on research on concepts which have been chosen by the ITER partners for their Test Blanket Module (TBM) studies. Progress on the conceptual design studies of the Japanese Water-cooled solid breeder (WCSB) TBM [91], and the Chinese Helium-cooled solid breeder (HCSB) [92] was presented. Special studies aimed at establishing the safety aspects of ITER TBMs against transient accident events such as Loss of Flow (LOFA) or Loss of Coolant (LOCA) accidents were discussed for the Japanese [91] and the two Chinese concepts [93], [94], with paper [93] also discussing environmental releases and decay heat at the end of experimental life. The end of life activation from the Dual Function Lithium Lead (DFLL) TBM is such that hands on recycling is possible after 100 years with the exception of the alumina components [93]. In-vessel LOCAs for all concepts lead to the predicted extinguishing of the ITER plasma, but the resultant pressure rises (in the 10s of kPa range) are well within the limits of the ITER Vacuum vessel (VV) and the inventory releases are small compared to ITER limits. The occurrence of a LOCA inside the TBM for the HCSB concept results in a very high pressure in the helium purge gas (7.3 MPa) within one second. Rupture of the TBM box and ingress into the ITER VV still results in only modest VV pressure increase and inventory release. On the other hand, in this concept, the tritium extraction system ex-vessel must be isolated from the TBM shortly after the accident to avoid over-pressurisation of the purge-gas loop.

Other aspects of the support research for the ITER TBM concepts were covered for: the pebble-bed [95] and the tritium recovery systems [96] of the Japanese WCSB; and the neutronics test of mock-ups of the European Helium-cooled Lithium Lead (HCLL) and Helium-Cooled Pebble Bed (HCPB) concepts, performed in the neutron-generator source at Frascati [97].

Corrosion reaction with the RAFM steel structure of materials within the blanket used as either neutron multipliers, or coolant or having a dual breeding/coolant function remains and important area of research. Advanced neutron multipliers with higher stability at high temperatures are a desirable pebble-bed component for DEMO. Beryllides such as $Be_{12}Ti$ and $Be_{12}V$ are promising candidates. Tests as part of the Broader Approach programme [85] have shown that Be-Ti and Be-V alloys are compatible with RAFM steels such as F82H. Growth rates of the reaction layer on F82H were ~ 1000x smaller than that of metal beryllium at the blanket operation temperature (see fig 32). These alloys remain rather brittle however, and fabrication of pebbles for a blanket is difficult, although large Be-Ti rods have been recently fabricated at Fz Karlsruhe. Corrosion of steels with static and flowing molten lithium and Flibe salt coolants/breeding materials has been studied [98], [99] in the Japanese programme. Exposure of RAFM steel to liquid Li induces depletion of carbon and a resultant transformation of the surface layer from the martensitic to the ferritic phase. Flowing coolant enhances this phase change.

Corrosion of RAFM by Flibe is induced by fluoridation and oxidation. The corrosion loss in both cases would be reduced by reducing the nitrogen levels in the Li and by avoiding dissimilar materials for the Flibe case. The corrosion rates measured were rather low (in the 10 -100 μm per year range) and are in general agreement with modelling, such as ref [100].

6 Reactor studies

Several reactor studies announced at previous IAEA FEC meetings gave progress updates at this meeting. There were new submissions on the Aries Compact Stellerator Design [101], and the Japanese Slim-CS, low aspect ratio tokamak [102], [103] and Large-Helical Device [104], [105] designs. The second Slim-CS submission addressed the challenging issue of lowering the divertor power loading in the 500 MW reactor from 70 $MW.m^{-2}$ to < 10 $MW.m^{-2}$. Of the factor 7 reduction, around a factor 3 comes from copious deuterium puffing in the divertor region (2 10^{23} atoms. s^{-1} –about twice the main chamber puff rate). The divertor plasma is detached at this level. The sensitivity to Argon fraction in the puff shows that 5% Ar in D_2 reduces the puff required to 10^{23}atoms.s^{-1}. At present the divertor codes used by the authors have not been linked up to main chamber confinement codes, to check if high plasma performance can be maintained.

Finally, one submission was made on a Fusion-Fission hybrid reactor concept from the Chinese programme [106]. This is based on a conservative tokamak device (R= 4m, a = 1m) with I_p=6.1MA, giving around 50 MW of fusion power at near unity fusion gain (Q~0.95). This is surrounded by a fission and breeder blanket. The inner blanket layer of fission material consists of depleted uranium and a mix of Minor Actinides (MA) such as would come after processing from the unloading of an end-of-life PWR fuel rod assembly. The mean energy gain from the sub-critical fissile blanket over a 5-year life (a nominal period between re-fuelling) is calculated at 79, giving an overall thermal power plant yield close to 4 GW. The outer tritium breeding layers contain Li-Pb breeder. The design is calculated to achieve a mean tritium breeding ratio of ~ 1.18 over the 5 year life.

7 Economics of Fusion

An interesting paper from Ward and Dudarev [107] compared the economic advantages of developing fusion materials to certain stages in terms of lifetime. The cost of electricity is simulated for a number of reactor concepts using the PROCESS code which combines the plasma performance as a function of machine size and plasma stability and confinement assumptions with a system approach to the issues like the power flow, thermodynamic efficiency and availability. The output predictions of the code crucially include the cost of electricity (coe). Part of the issue of availability is the necessary intervals between machine shutdowns to replace the divertor and first-wall blanket systems. The modelled coe depends strongly in an

inverse manner on machine availability ($A^{-0.6}$), and also inversely with thermodynamic efficiency of the blanket coolant – steam raising circuit ($\eta_{th}^{-0.4}$). These have a much stronger influence on the coe than the materials development issues, which plateau out in their ability to reduce the coe after a certain level is reached. Fig 33 shows the coe as a function of machine availability and thermodynamic efficiency. In the case of materials development, fig 34 shows that the coe is reduced as the lifetime of the first wall blanket steels are increased. It shows that there is a cost advantage in developing materials to the 150 dpa range, but not much higher, and that, for the economic use of a first of a kind system such as DEMO, a material surviving 50 dpa would be sufficient

8 Conclusions

The papers submitted in the ITER Activities, Fusion Technology and Economics area show a continuing strong world-wide programme.

The fusion tokamak community has now been joined by the world's first Nb_3Sn superconducting coil machine in KSTAR. Construction proceeds on the W7X stellarator and two 'ITER-generation' fusion research machines in FAST and NHTX have been proposed.

ITER has seen a concentrated and successful physics effort to improve the margins of its start up and burn for the standard Q=10, 15 MA scenario. The ramp-down remains challenging. Vertical stability is improved with the new in-vessel coil proposals, which have been combined into an ELM-mitigation proposal.

The ITER Technology programme is making progress. There has been significant progress with qualifying the TF superconductor strand for ITER and removing the previous development uncertainties. The PF conductor has been successfully characterised and NbTi conductor behaviour validated. Progress continues on the Heating and Current Drive systems with the highlights being the achievement of the ITER parameters for the Japanese 170 GHz gyrotron and the launch of the testing of the ITER-like ICRF antenna in JET. Concepts have been chosen for the ITER Negative Ion Neutral Beam source and accelerator stack. Fuelling remains a 'Cinderella' subject, in spite of its crucial importance, but progress is made within the US programme for ITER Diagnostics for ITER are now concentrating on the basic topics of dust and tritium detection/measurement for licensing purposes, and on the survivability of the first wall mirrors.

The simulation of tungsten first wall shows survivability in a reactor environment, and tests of tritium retention in tungsten show encouragingly low values.

There is considerable activity in RAFM steels and SiC/SiC composites, stimulated by the Broader Approach programme (which has also seen the design of IFMIF progress). A possible operational route for survivability of a first wall in RAFM steel

is shown to be operation at 350° - 450°C followed by annealing at 550°C before cooldown. RAFM steel corrosion and reaction of beryllium bearing neutron alloys and liquid and molten salt breeders is found to be relatively low. The NITE-derived SiC/SiC looks to have significant materials advantages over other variants.

Concepts for the ITER TBM continue to be the focus stimulating technical work, including safety analyses, in the blanket research field.

Reactor concept work continues, but without any new concepts being presented, and, for the moment, a lull in the work in Europe.

Economics studies are pointing up the relative merits of materials performance goals, especially the law of diminishing returns in high achievement of radiation damage performance.

Acknowledgements

The author is pleased to acknowledge many stimulating and informative conversations with presenters at the Geneva meeting and since the conference. Any errors contained within are entirely due to my own limitations.

The views expressed herein are personal, and do not necessarily represent the views of my Association, nor of the relevant bodies, the UK Engineering and Physical Sciences Research Council, or the European Communities, who fund the work of the UKAEA Euratom Fusion Association.

References

References presented below as papers at this conference are available online at http://www-naweb.iaea.org/napc/physics/FEC/FEC2008/html/index.htm.

[1] Bak J S et al., '*Overview of Recent Commissioning Results of KSTAR*' paper FT/1-1.

[2] Hanada K et al.*, 'Physical Design of MW-class Steady-state Spherical Tokamak, QUEST'* paper FT/P3-25.

[3] Kim Y S et al., *'Commissioning Results of the KSTAR Cryogenic System'* paper FT/P3-1.

[4] Oh Y K et al.*, 'Commissioning Results of the KSTAR Superconducting Magnet System for the First Plasma Operation'* paper FT/P3-2.

[5] Park M et al.,*'Operation Results of KSTAR Integrated Control System for First Plasma'* paper FT/P3-3.

[6] Yang H L et al., *'KSTAR Assembly and Vacuum Commissioning for the 1st Plasma'* paper FT/P3-4.
[7] Garin P et al., *'The IFMIF/EVEDA Project: Outcome of the first Engineering Studies'* paper FT/1-2.
[8] Klinger T et al., *'The construction of the Wendelstein 7-X stellarator'* paper FT/1-4.
[9] Tazhibayeva I et al., *'KTM Tokamak Project. Present and Future Activity'* paper FT/P3-7.
[10] Pizzuto A et al., '*The Fusion Advanced Studies Torus (FAST): a Proposal for an ITER Satellite Facility in Support of the Development of Fusion Energy'* paper FT/1-5.
[11] Goldston R J et al., *'An Experiment to Tame the Plasma Material Interface'* paper FT/P3-12
[12] Cucchiaro A et al., *'Load Assembly Design of the FAST Machine'* paper FT/P3-5.
[13] Tsitrone E at al., J Nucl Matls 363 (2007) 12.
[14] Valanju P et al., Phys Plasmas 16 (2009) 056110.
[15] Holtkamp N et al., '*Status of the ITER Design*', paper OV/2-1.
[16] Alejaldre C et al., *'ITER on the Way to Become the First Fusion Nuclear Installation'* paper IT/1-1.
[17] Hawryuluk R J et al., Nucl Fusion 49 (2009) 065012..
[18] Sips A C C et al., Nucl Fusion 49 (2009) 085015..
[19] Jackson G L et al., '*Simulating the ITER Plasma Startup Scenario in the DIIID tokamak*', paper IT/P7-2.
[20] Kessel C E et al., *'Development of ITER 15MA ELMy H-mode scenario*', accepted for publication in Nuclear Fusion (2009).
[21] Kukushkin A S et al., *'Analysis of Performance of the Optimized Divertor in ITER*'., paper IT/P6-15.
[22] Portone A et al., *'ITER Plasma Vertical Stabilization'* paper IT/2-4Ra.
[23] Humphreys D A et al., Nucl Fusion 49 (2009) 075008.
[24] Loarte A et al., *Progress in the ITER Physics Basis,* Nuclear Fusion 47 (2007) S203.
[25] Loarte A et al., *'Power and particle fluxes at the plasma edge of ITER : Specifications and Physics Basis'* paper IT/P6-13.
[26] Thomas P R et al., *'ELM physics and ELM mitigation in ITER'***,** paper IT/1-5.
[27] Tereshin V I et al., *'Simulation of ITER Transient Heat Loads to the Divertor Surfaces with Using the High Power Quasi-Steady-State Plasma Accelerator'***,** paper IT/P6-12.
[28] Baylor L et al., Nucl Fusion 49 (2009) 085013.
[29] Compan J et al., J Nucl Materials 386-388 (2009) 797-800.
[30] Becoulet, M et al., Proc 21st IAEA FEC, Chengdhu, 2006, paper IT/P1-29.
[31] Whyte D G F et al., *'Studies of Requirements for ITER Disruption Mitigation Systems'*, paper IT/P6-18.
[32] Lowry C et al., *'Progress in Design and R&D on ITER Plasma Facing Components'* , paper IT/1-4.
[33] Chen J M et al., *'ITER first wall fabrication technology in China'*, paper IT/P7-10.
[34] Weng P et al., *'Results of ITER Superconducting Magnet R&D'*, paper IT/1-3.
[35] Bruzzone P et al., Nuclear Fusion 49 (2009) 065034.
[36] Zanino R et al., *'EU Contribution to the Test and Analysis of the ITER Poloidal Field Conductor Insert (PFCI)'*, paper IT/P7-14.

[37] Abe K et al., IEEE Trans App Sup (16)2, 807-810, (2006)..
[38] Humer K et al., Fus Eng and Design 84 (2009) 960-963.
[39] Costley A E et al., *'Measurement Requirements and the Diagnostic System on ITER: Modifications Following the Design Review'*, paper IT/P6-21.
[40] Donne A J H et al., *'Key R&D activities for ITER Diagnostics'*, paper IT/P6-20.
[41] Skinner C H et al., *'Electrostatic Dust Detection and Removal for ITER'*, paper IT/P6-26.
[42] Litnovsky A et al, Nuclear Fusion 49 (2009) 075014.
[43] Mukhin E et al., '*Research and Development of Optical Diagnostics for ITER',* accepted for publication in Nuclear Fusion (2009).
[44] Ogawa H et al., '*Research and Development of Optical Diagnostics for ITER*', paper IT/P6-23.
[45] Walsh M J et al., *'Performance Evaluation of ITER Thomson Scattering Systems'*, paper IT/P6-25.
[46] Brooks J N and Allain J P, Nucl Fusion 48(2008) 045003.
[47] De Temmerman G et al., J Appl Phys 102 (2007) 083302.
[48] Sakamoto K et al., *'Progress in ITER Heating and Current Drive System'*, paper IT/2-1.
[49] Kasugai et al., *' Demonstration of 1MW quasi-CW operation of 170GHz Gyrotron and Progress of EC Technology for ITER'*, accepted for publication in Nuclear Fusion (2009).
[50] Denisov G G et al., Nucl Fusion 48 (2008) 054007.
[51] Rzesnicki T et al., '*Experimental Investigations on the Pre-Prototype of the 170 GHz, 2 MW Coaxial Cavity Gyrotron for ITER'*, paper FT/3-1Rc.
[52] Gantenbein G et al., *'Experimental Results of Series Gyrotrons for the Stellarator W7-X'*, paper FT/P2-24.
[53] La Haye R J et al., Nuclear Fusion 49 (2009) 045005.
[54] Sakamoto K et al., Proc 21st IAEA FEC, Chengdhu, 2006, paper IT/2-4Rc.
[55] Piosczyk B et al., Proc 21st IAEA FEC, Chengdhu, 2006, paper IT/2-4Ra.
[56] Nightingale M P S et al., *'RF and Mechanical Design of the ITER Ion Cyclotron Resonance Frequency Antenna'*, paper IT/P7-6.
[57] Dumortier P et al., *'Preparing ITER ICRF: Test of the Load Resilient Matching Systems on an Antenna Mock-up'*, paper IT/P7-8.
[58] Vulliez K et al., *' Validation of the Load-Resilient Ion Cyclotron Resonance Frequency Antenna Concept on Tore Supra Plasmas'*, paper FT/4-5Rb.
[59] Nightingale M P S et al., *' Development of the JET Ion Cyclotron Resonance Frequency Heating System in Support of ITER'*, paper FT/4-5Ra.
[60] Wukitch S J et al., '*Ion Cyclotron Antenna Impurity Production and Real Time Matching in Alcator C-Mod '*, paper EX/P6-23.
[61] Gunn J P et al., '*Suprathermal electron beams and large sheath potentials generated by RF-antennae in the scrape-off-layer of Tore Supra*', submitted to Nucl Fusion (2008).
[62] Bobkov V et al., '*ICRF Antenna Operation with full W-wall in ASDEX-Upgrade*',paper EX/P6-31.
[63] Fantz U et al., *'Physical Performance Analysis and Progress of the Development of the Negative Ion RF source for the ITER NBI System'*, paper IT/P7-9
[64] Kashiwagi M et al., Nucl Fusion 49 (2009) 065008 .

[65] Watanabe K et al., Nucl Fusion 49 (2009) 055022.
[66] Dremel M et al., Nucl Fusion 49 (2009) 075035.
[67] Oikawa T et al., *'Benchmarking of Neutral Beam Current Drive Codes as a Basis for the Integrated Modeling for ITER'*, paper IT/P6-5.
[68] Hoang J et al., Nucl Fusion 49 (2009) 075001.
[69] Callis R W et al., *'Alternate Concepts for Generating High Speed DT Pellets for Fueling ITER'*, paper FT/P2-23.
[70] Polevoi A R et al., Nucl Fusion 43 (2003) 1072.
[71] Baylor L R et al., Nucl Fusion 47 (2007) 443.
[72] Norajitra P et al., *'Status of development of the EU He-cooled divertor for DEMO'*, paper FT/P3-16.
[73] Lyublinski I et al., *'Main Results and Prospects of Lithium Capillary – Porous System Investigation as Tokamak Plasma Facing Material'*, paper FT/P2-15.
[74] Brooks J N et al., Nucl Fusion 49 (2009) 035007.
[75] Doerner R P et al., Nucl Fusion 49 (2009) 035002.
[76] Roth J et al., '*A new look at the specification of ITER plasma wall interaction and tritium retention*', paper IT/P6-16.
[77] Zohm H et al., published in this issue of Nuclear Fusion.
[78] Kallenbach A et al., '*Non-boronised Operation of ASDEX-Upgrade with Full-Tungsten Plasma Facing Components*', paper EX/9-2.
[79] Doerner R P et al, J Nucl Mater 363-365 (2007) 32.
[80] Tokitani M et al., J Nucl Mater 337-339 (2005) 937.
[81] Wright G M et al., *'Hydrogenic retention of high-Z refractory metals exposed to ITER divertor relevant plasma conditions'*, paper FT/4-2Rb.
[82] Philipps V et al., *'Development of wall conditioning and tritium removal techniques in TEXTOR for ITER and future fusion devices'*, paper FT/4-2Ra.
[83] Ezato K et al., *'Provisional Procurement Activity and R&D's on Divertor HHF Components in JADA'*, paper IT/P7-17
[84] Escourbiac F et al., *'Definition Of Workable Acceptance Criteria For The ITER Divertor Plasma Facing Components Through Systematic Experimental Analysis'*, paper FT/P2-21.
[85] Nishitani T., *' Fusion technology development for DEMO in the Broader Approach activities'*, paper FT/1-3.
[86] Garganidze E et al., *'Mechanical Properties of Reduced Activation Ferritic/Martensitic Steels after High Dose Neutron Irradiation'*, paper FT/P2-1.
[87] Jitsukawa S et al., *'Irradiation Effects on Reduced Activation Ferritic/Martensitic Steels-Mechanical Properties and Modeling*', submitted to Nuclear fusion (2008).
[88] Materna-Morris E et al., *'Microstructure and tensile properties in reduced activation 8-9% Cr steels at fusion relevant He/dpa ratios, dpa rates and irradiation temperatures'*, paper FT/P2-2.
[89] Oksiuta Z and Baluc N, Nucl Fusion 49 (2009) 055003
[90] Nozawa T et al., *'Evaluation on Failure Resistance to Develop Design Basis for Quasi-Ductile Silicon Carbide Composites for Fusion Application*', paper FT/P2-17.
[91] Tsuru D et al., Nucl Fusion 49 (2009) 065024
[92] Feng K M et al., *'Overview of Design and R&D of solid breeder TBM in China'*, paper FT/P2-9.

[93] Chen H et al., Nucl Fusion 49 (2009) 075040
[94] Liu H and Feng K, *'Thermal-hydraulic safety study of Chinese helium cooled solid breeder test blanket module for ITER'*, paper FT/P2-8.
[95] Tanigawa H et al., Nucl Fusion 49 (2009) 055021
[96] Kawamura et al., Nucl Fusion 49 (2009) 055019
[97] Fischer U et al., Nucl Fusion 49 (2009) 065009
[98] Muroga T et al*., 'Compatibility of Reduced Activation Ferritic/Martensitic Steels with Liquid Breeders'* paper FT/4-3Rb.
[99] Nagasaka T et al*., 'Progress in Flibe corrosion study toward material research loop and advanced liquid breeder blanket'* paper FT/P2-4.
[100] Sannier J et al., proc 16th SOFT, London (1990), vol 1, 901 (North-Holland , Elsevier, 1991).
[101] Najmabadi F et al., *'Compact Stellarator Power Plants – Prospects, Technical Issue, and R&D Directions'*, paper FT/P3-13.
[102] Tobita K et al., Nucl Fusion 49 (2009) 075029
[103] Kawashima H et al., Nucl Fusion 49 (2009) 065007
[104] Imagawa S et al., Nucl Fusion 49 (2009) 075017
[105] Mitarai O et al., *'The low temperature and high density ignition in the helical reactor FFHR2m based on LHD experiments'*, submitted to Nuclear Fusion (2009)
[106] Wu Y et al., *'The fusion-fission hybrid reactor for energy production-a practical path to fusion application'*, paper FT/P3-21.
[107] Ward D J and Dudarev S L, '*Economic Consequences of Fusion Materials Development*', paper SE/1-1.

Coil	Base line	I, kA	B, T	N
PF2	2001	41	4	106
	2008	55 / 55	4.8 / 5.0	115.2
PF5	2001	45	5	216.8
	2008	52 / 33	5.7 / 6.0	216.8
PF6	2001	45	6	424.4
	2008	52*/41*	6.8*/7.0*	459.4

(a)

Conductor version		SC: Cu	A mm²		SC strand
			SC	Cu	
PF2 3, 4	2001	1:6.9	45.3	430.8	864
	2008	1:2.3	90.3	424.7	720
PF5	2001	1:4.4	80.5	422.3	1080
	2008	1:2.3	144.8	370.5	1152

(b)

Table 1: (a) New ITER PF coil requirements for 15 MA scenario (* indicates performance with sub-cooling.
(b) Main changes in PF2-5 conductors.

Particle type	Particle flux to the entrance of diagnostic module particles/(m^2*s)	Resulting atom flux to the surface of the first mirror particles/(m^2*s)	Reduction factor
D-T charge exchange atoms (full energy spectrum)	7.21×10^{20}	3.96×10^{18}	182
D-T charge exchange atoms (>10 eV spectrum)	2.56×10^{20}	1.29×10^{18}	198
D-T ions from plasma edge	3.59×10^{20}	9.10×10^{17}	391
He charge exchange atoms (full energy spectrum)	6.50×10^{17}	4.26×10^{15}	153
He charge exchange ions (from plasma edge)	1.80×10^{19}	4.55×10^{16}	395
Be ions (sputtered from Be wall)	1.47×10^{19}	5.81×10^{16}	253
W ions (sputtered from alternative W wall)	8.71×10^{16}	2.68×10^{13}	3250

Table 2: Attenuation of the particle fluxes towards the first mirror of the ITER Core MSE system as modelled in [46], quoted in ref [42].

Wall surface	Sputtered current[a] atoms/s	Erosion rate[b] m/s	Erosion lifetime, 1 mm surface @1% duty factor years
Beryllium	$1.9\ x10^{22}$	$3.2\ x10^{-10}$	~10
Iron (stainless steel)	$1.0\ x10^{21}$	$5.0\ x10^{-11}$	~60
Tungsten	$5.6\ x10^{19}$	$1.8\ x10^{-12}$	~1700

[a] for outer first wall, scaled from lower-half outer-wall results.
[b] rate approximately spatially uniform; not including local peaking, if any, due to CX from gas puffing

Table 3: ITER outer first wall sputtering rates from [74] for reference Q=10 ELMy H-mode with convective plasma edge regime.

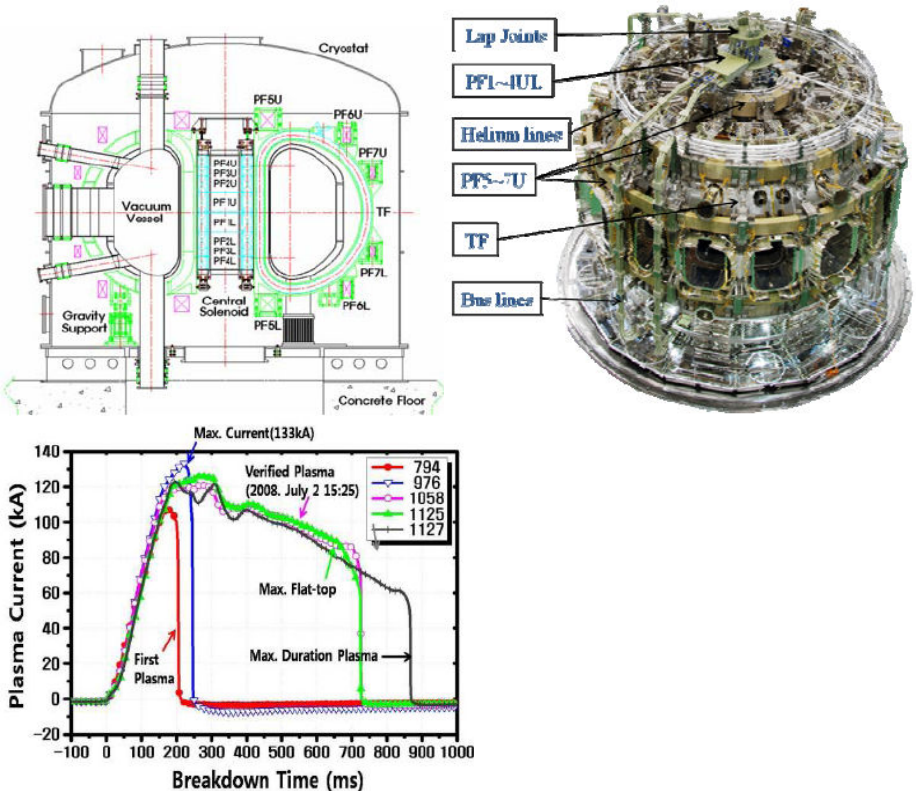

Fig 1: (a) Cross-section of KSTAR coil system
(b) View of the KSTAR coil system with cryostat connections.
(c) Plasma current commissioning history for 2008 operation.

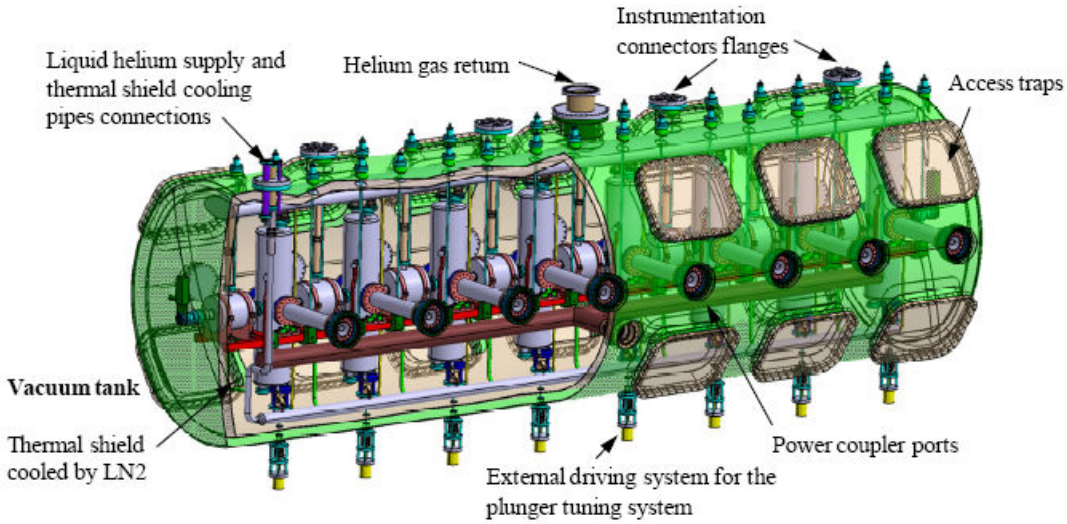

Fig 2: General view of the first cryomodule of the IFMIF Drift Tube Linac (DTL) – to be tested during the EVEDA programme.

(a)

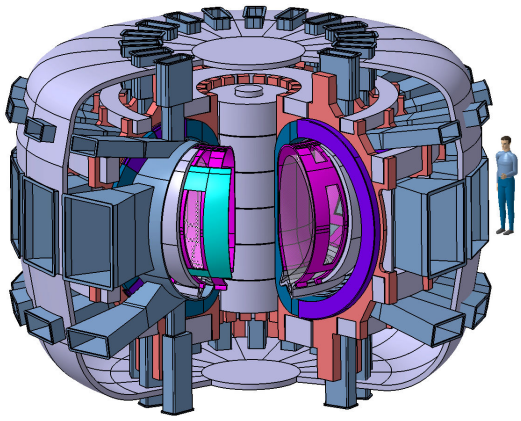

(b)

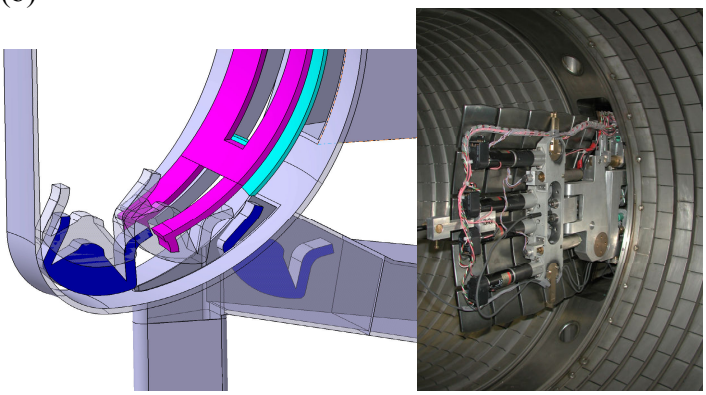

Fig 3: (a) Load Assembly design for the FAST proposal
(b) Detail of the Remote handling concept for replacement of tungsten divertor modules.

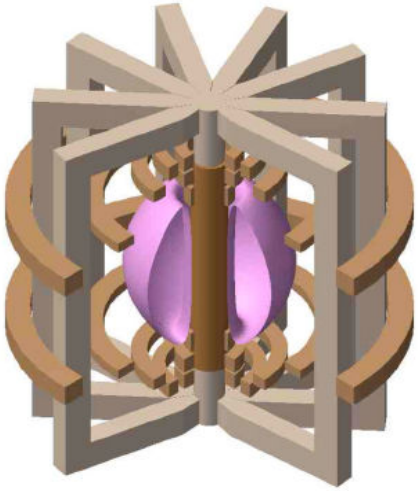

4(a)

4(b)

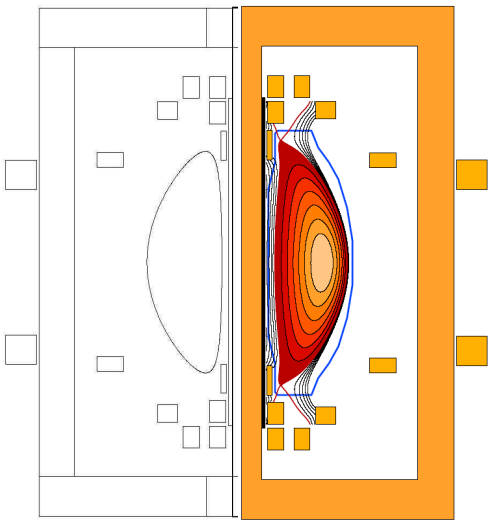

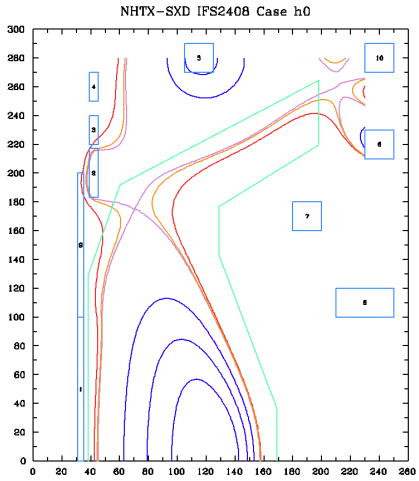

4(c)

Fig 4: (a) Load Assembly concept for NHTX; (b) NHTX equilibrium
(c) Equilibirium of 'Super-X' expanded divertor concept for NHTX.

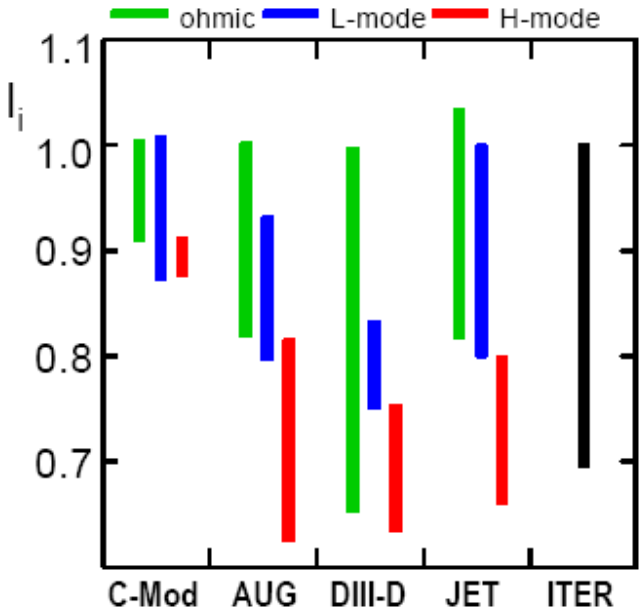

Fig 5: Range of l_i achieved during the current rise of the ITER-like discharges in the various devices for ohmic (green), L-mode (blue) and H-mode (red). The ITER range for l_i is shown in black.

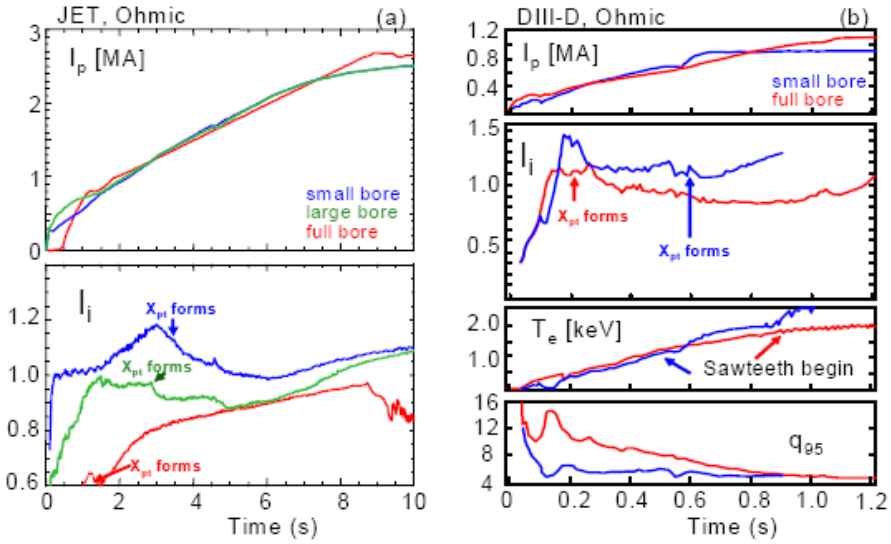

Fig 6: Evolution of plasma inductance l_i for rise phases of JET (a) and DIID (b). The evolution of the originally envisaged small bore ITER start up is shown in blue. Full bore ramp up discharges are indicated in red. The green JET trace is a large bore limiter case with an X-point formation delayed with respect to the red trace discharge.

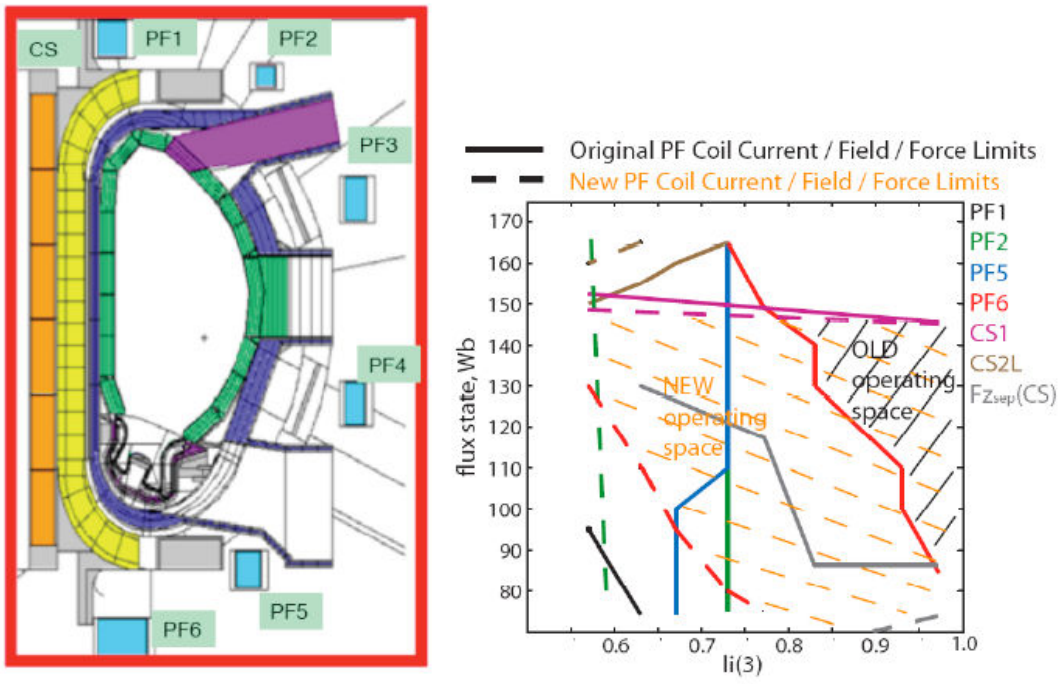

(a) (b)

Fig 7: (a) Cross-section of ITER Poloidal field set and central solenoid .
(b) Flux state vs l_i diagram showing comparison of OLD and NEW operating spaces at 15 MA.

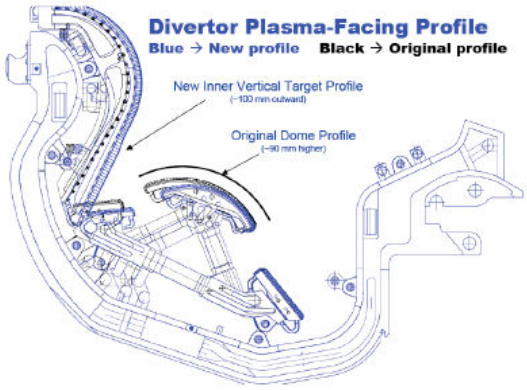

Fig 8: Details of the proposed changes to the ITER Divertor dome to improve the full-bore plasma capability.

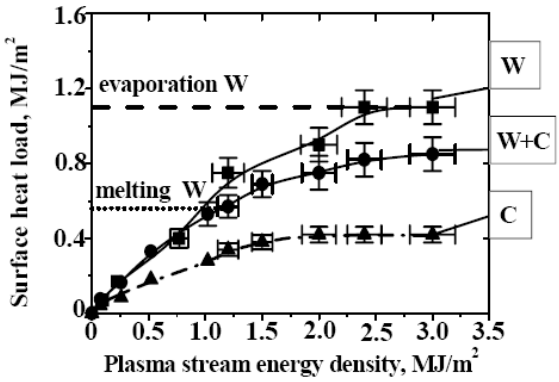

(a)

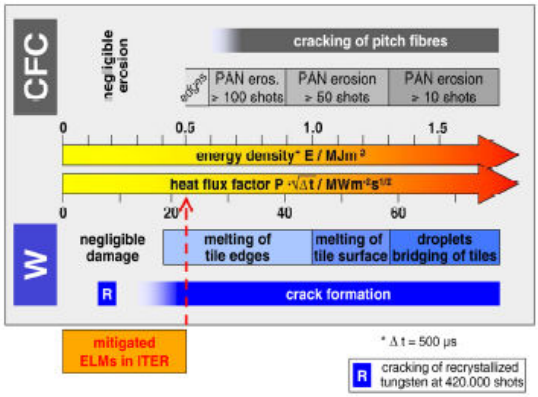

(b)

Fig 9: (a) Heat loading achieved in the plasma-stream damage measurements on tungsten and CFC at the QSPA Kh-50 plasma accelerator at the Kharkov Institute of Plasma Phyiscs [27]. Note the effects of vapour shielding in limiting the surface heat load.

(b) Overview of the damage to CFC and tungsten divertor targets by ELMs. From ref [26] quoting the results in paper [29]

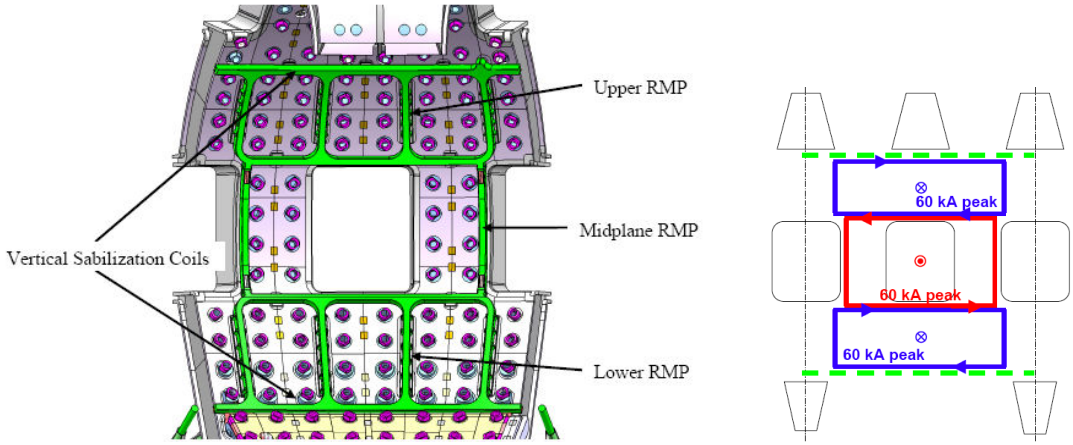

Fig 10: Proposed design for the ELM mitigation and vertical stability coils for ITER.

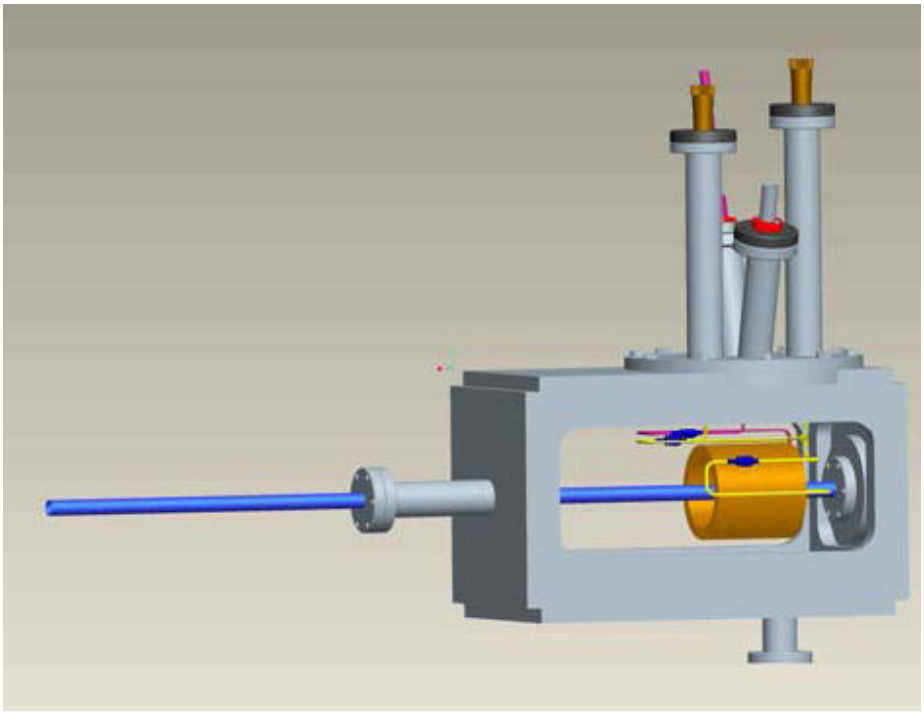

Fig 11: CAD model of the large diameter pipe-gun device being developed for mitigating disruptions with large 16 mm diameter pellets that are shattered before entering the plasma.

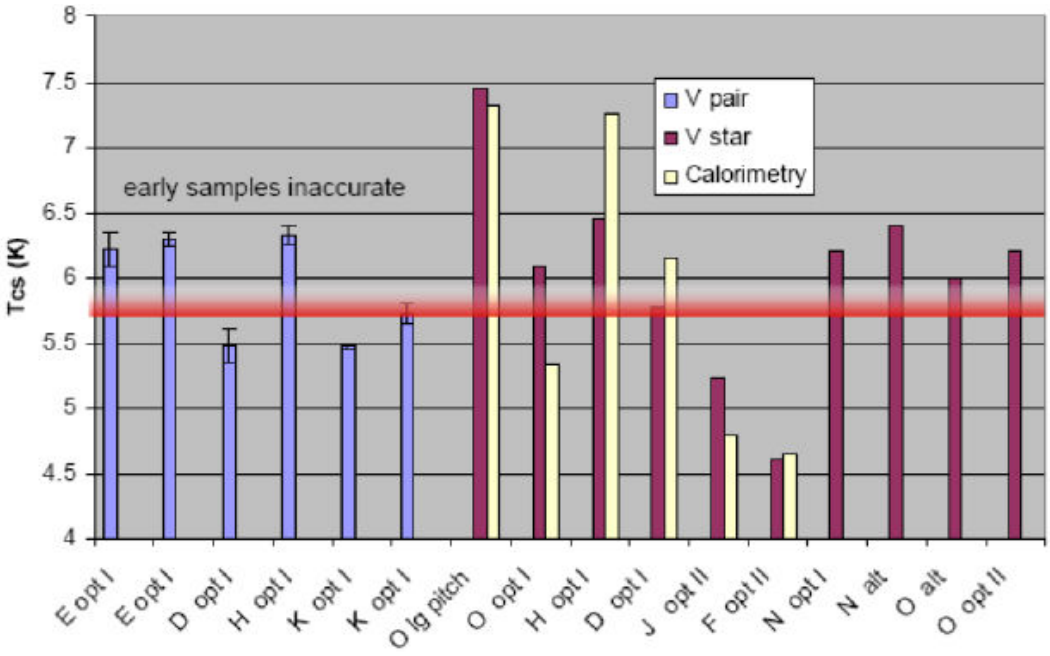

Fig 12: Current sharing temperature results (after 1000 cycles) of the Nb_3Sn conductor samples in Sultan. The 'V pair' for early samples refers to the electrical measurements before the instrumentation was changed, whilst 'V star' is post-improvement.

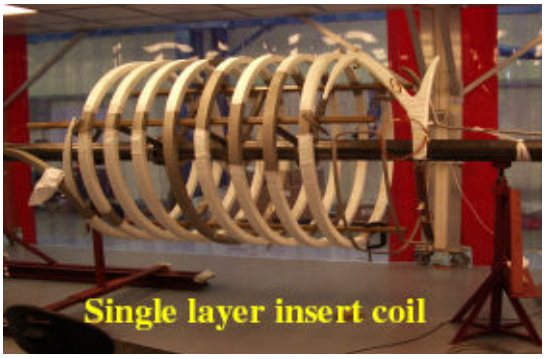

(a) (b)

Fig 13: (a) Poloidal Field Coil Insert (PFCI) test solenoid
(b) Installation of PFCI at CSMC Facility, Naka, Japan.

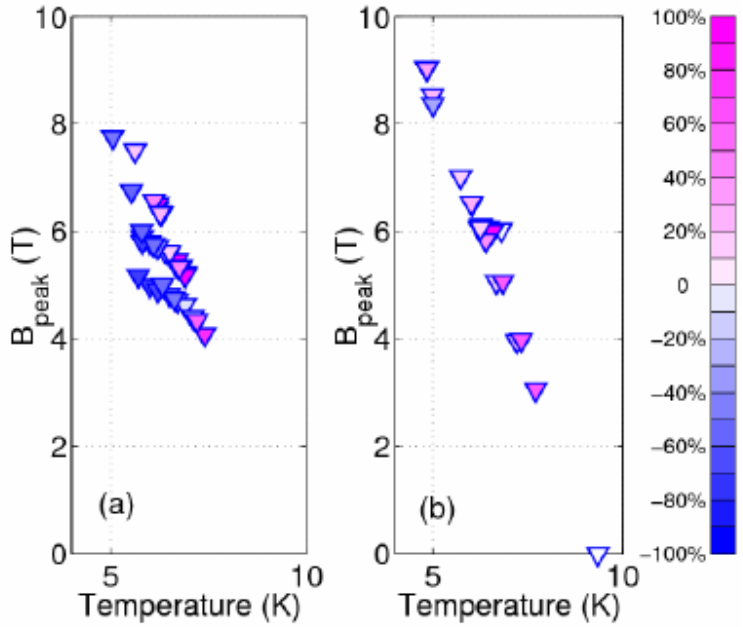

Fig 14: Summary of DC performance of short samples of PF conductor (left hand graph) and PFCI conductor (right hand graph). The graphs compare the critical conductor current (I_C) at the measure peak field (B_{peak}). The relative deviation is indicated in the symbol sharing between the measured critical quench current and that resulting from all strands carrying the current equally, ie: deviation = $(I_c - I_c^{strand} x\ n_{strands})/I_c$

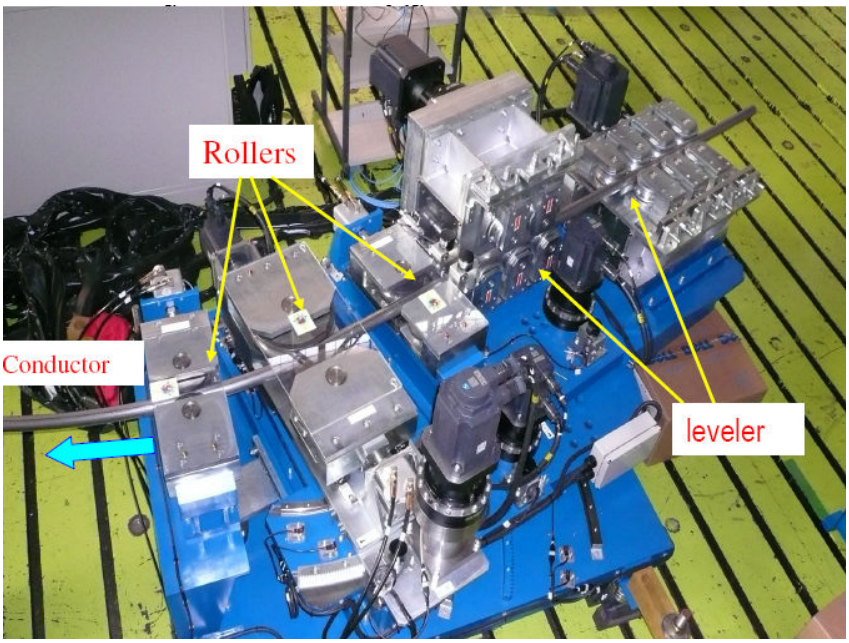

Fig 15: High-accuracy automatic winding head developed by the Japanese Domestic Agency for ITER TF coils.

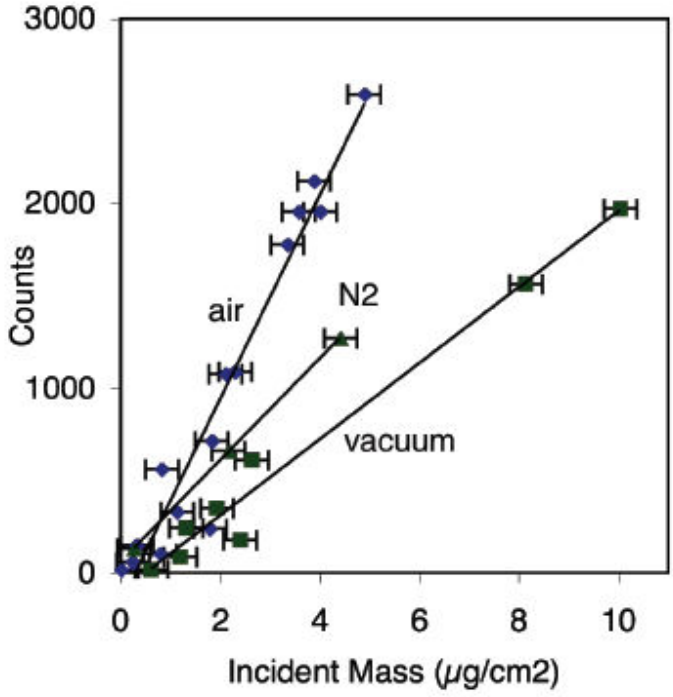

Fig 16: Response of a 51x51 mm conducting grid to carbon microparticles in air (diamonds), nitrogen (triangles) and vacuum (squares). Lines are least-squares fits to data [41] and references therein..

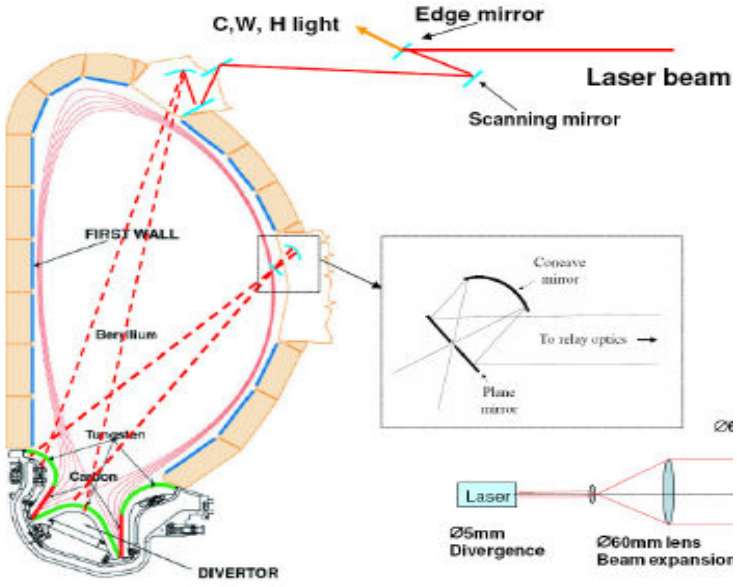

Fig 17: TEXTOR-team proposed LIB system with ablation and desorption spectroscopy and Mie-Rayleigh scattering.

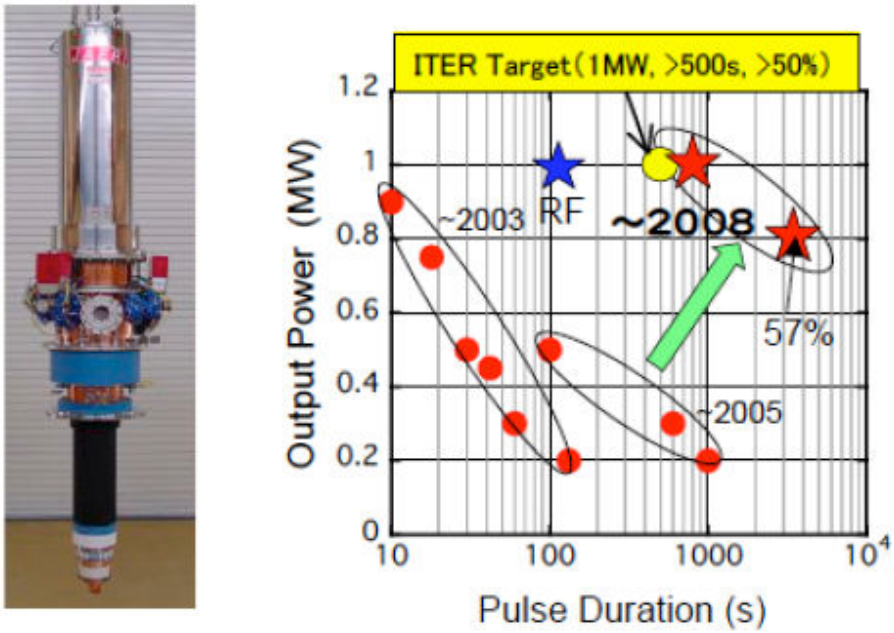

(a) (b)

Fig 18: (a) Japanese prototype 170 GHz gyrotron for ITER ECRH system.
(b) Progress of Japanese ITER gyrotron in terms of achieved power and pulse length. Red dots refer to previous record levels, red star shows the performance reached in 2008 [49]. The blue star shows the best performance from the Russian ITER gyrotron for comparison.

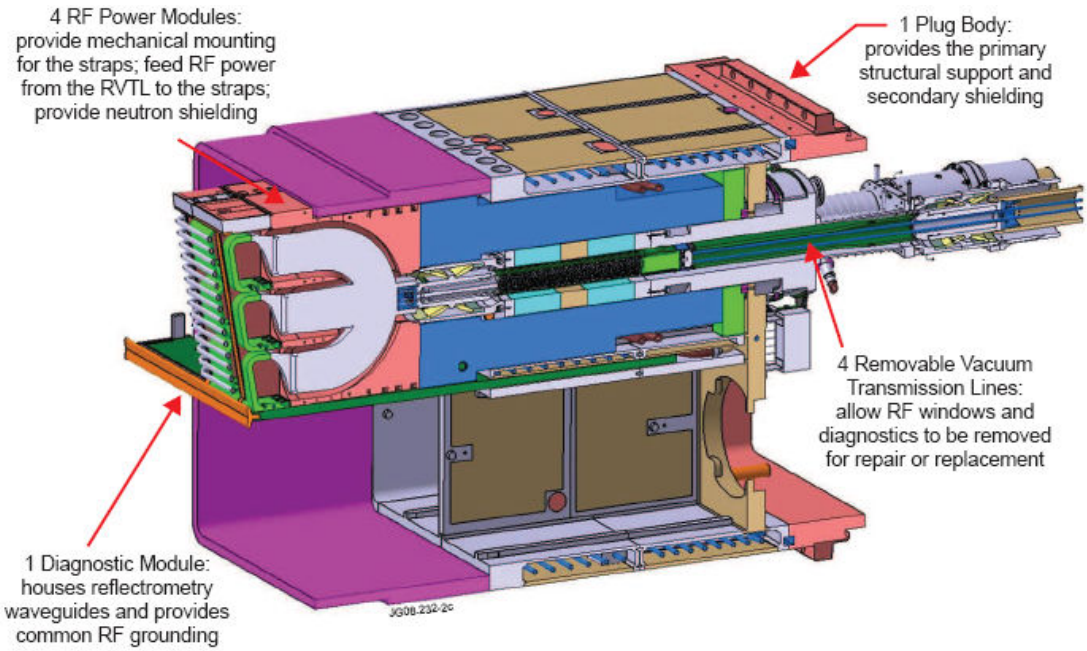

Fig 19: Section through the ITER ICRF Antenna with one RF power module and Removable Vacuum Transmission Line (RVTL) installed.

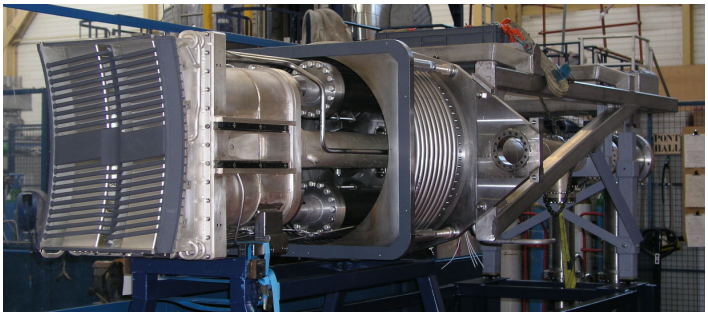

(a)

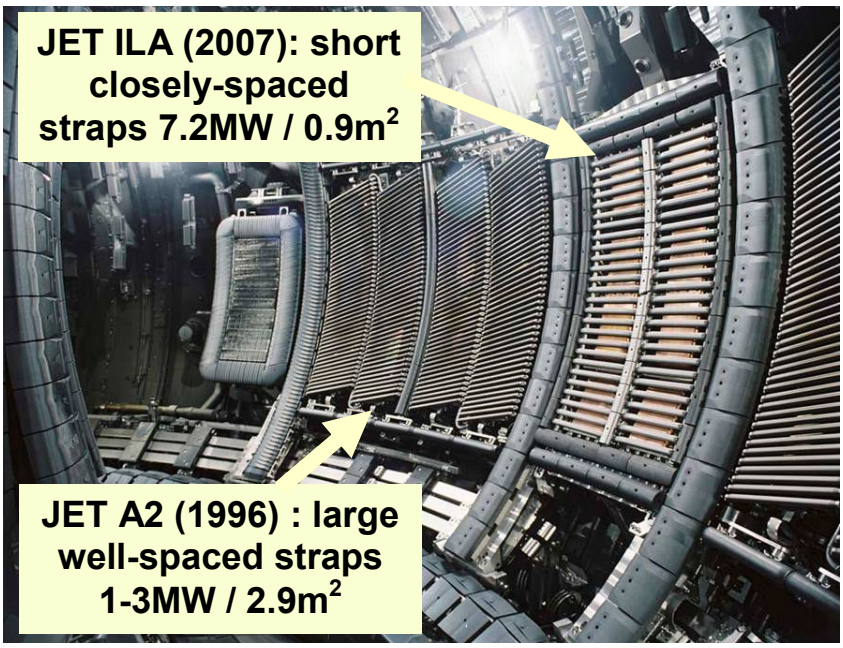

(b)

Fig 20: ITER-like ICRH antennae under test on present generation tokamaks.
(a) ITER-like Prototype (ILP) before installation on Tore Supra.
(b) JET ITER-like Antenna (ILA) after installation, compared to previous generation (A2) JET Antenna.

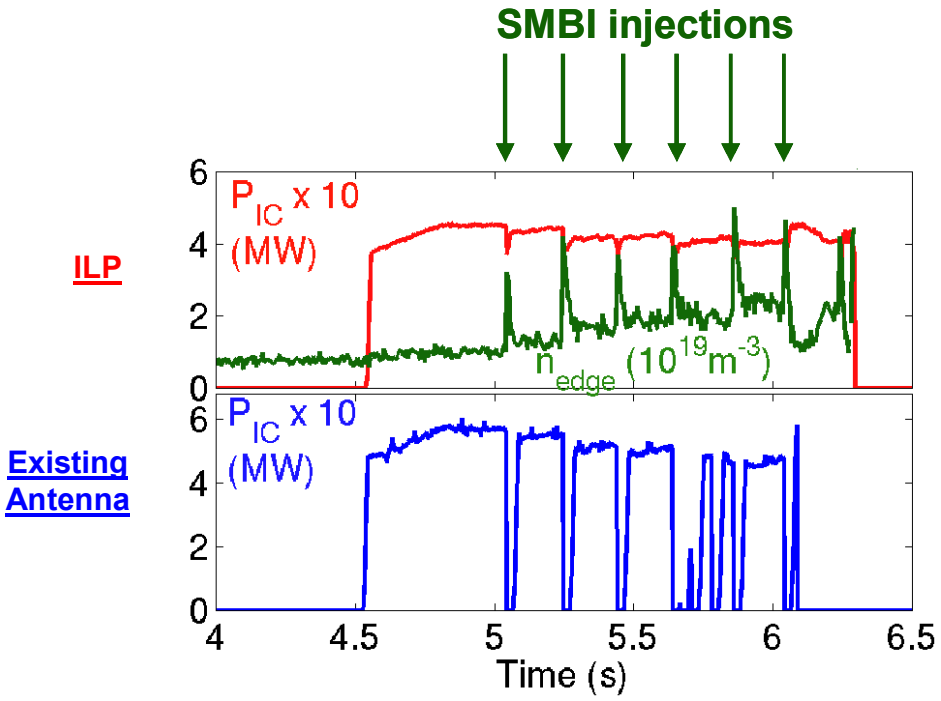
SMBI injections
ILP
Existing Antenna
P_IC x 10 (MW)
n_edge (10^19 m^-3)
P_IC x 10 (MW)
Time (s)

(a)

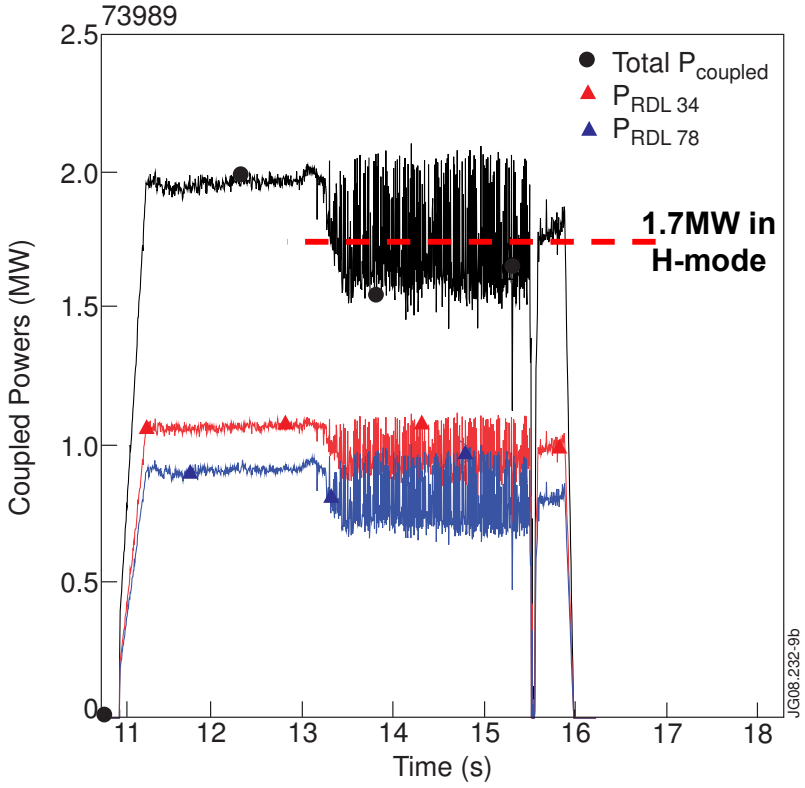
73989
Total P_coupled
P_RDL 34
P_RDL 78
1.7MW in H-mode
Coupled Powers (MW)
Time (s)
JG08.232-9b

(b)

Fig 21: Performance of ITER-like ICRH antenna under plasma conditions.
(a) Tore-Supra ILP (top trace) shows continued ability to maintain level of power coupled to plasma during Supersonic Molecular Beam Injection (SMBI) whilst other antenna trips (bottom trace).
(b) JET ILA coupling 1.7 MW into an ELMy-H-mode (transition at 13.5s) from half the antenna. This corresponds to ~ 3.8 $MW.m^{-2}$. During the L-H transition, the plasma moves by ~ 1 cm from the plasma. Again the antenna is able to continue to couple power.

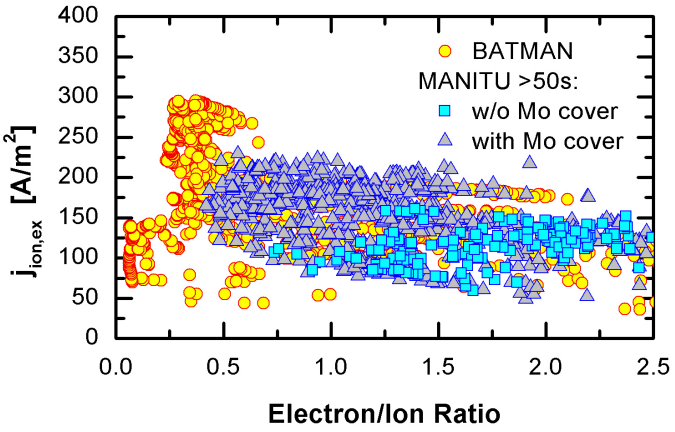

Fig 22: Plot of negative deuteron ion extracted current in low energy extracted negative beams as a function of electron to ion ratio in the beam from the RF negative ion source at IPP Garching, Plot shows the improvement in reaching the ITER target for current density (200 $A.m^{-2}$) at an acceptably low electron:ion ratio (<1) when molybdenum cover on the source copper surface is employed.

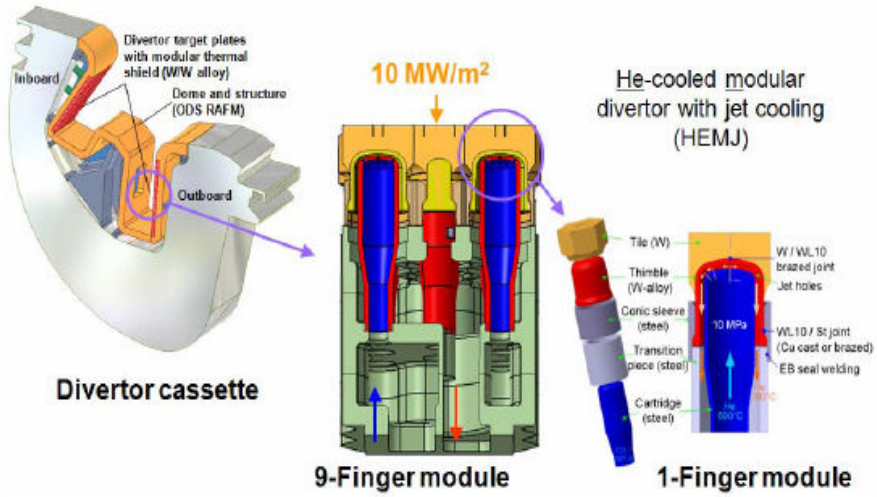

Fig 23 (a) Helium-cooled Multi-jet (HEMJ) divertor concept design.

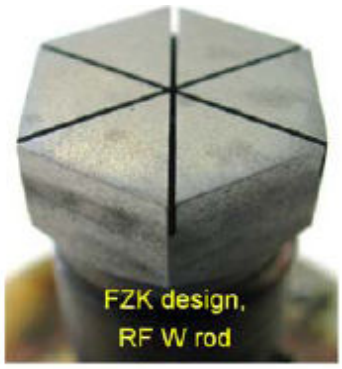

#25 – tested

- 10 cycles at ~ 10 MW/m² (sharp ramp);
100 cycles at ~11 MW/m² (sharp ramp);
10 cycles at ~11.5 MW/m² (sharp ramp),
- good performance, no any damages
- available for further tests

Fig 23 (b): HEMJ thimble after cycling power loading tests up to 11.5 MW.m^{-2}

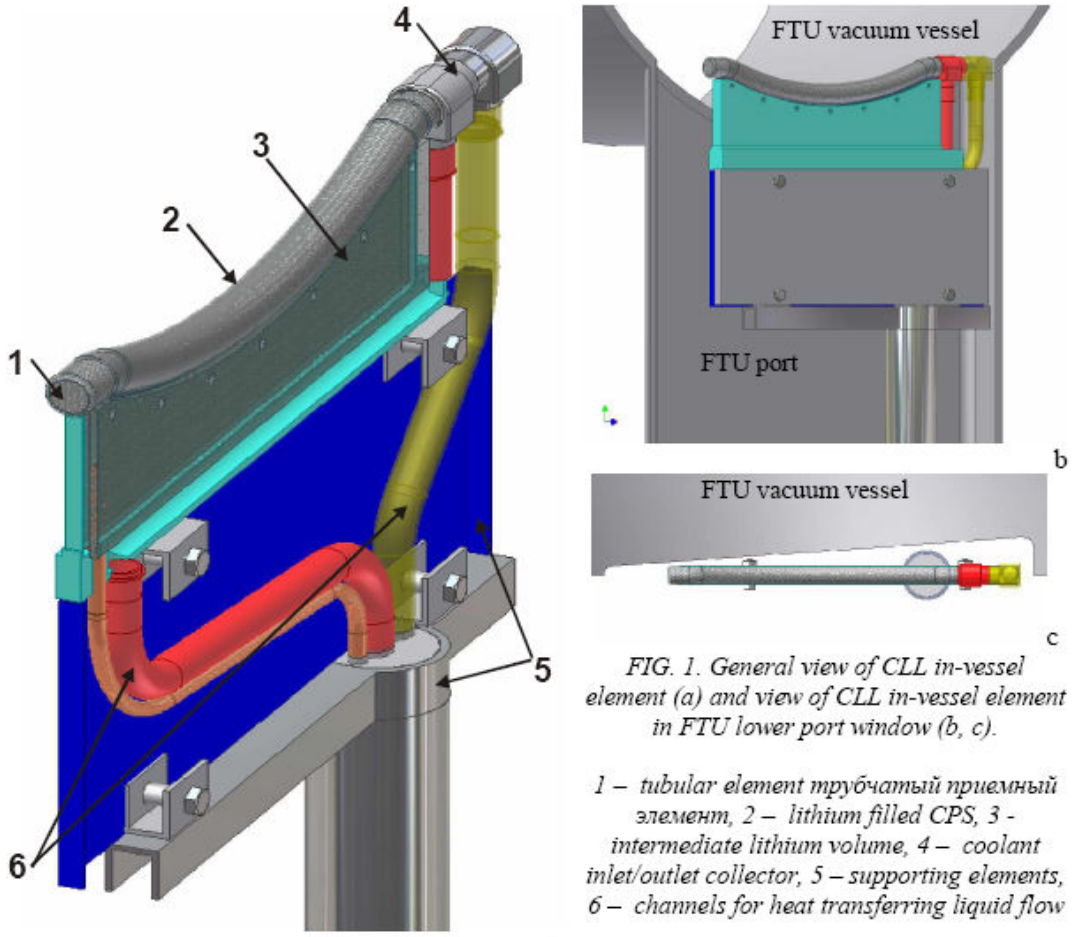

FIG. 1. General view of CLL in-vessel element (a) and view of CLL in-vessel element in FTU lower port window (b, c).

1 – tubular element трубчатый приемный элемент, 2 – lithium filled CPS, 3 - intermediate lithium volume, 4 – coolant inlet/outlet collector, 5 – supporting elements, 6 – channels for heat transferring liquid flow

Fig 24; (a) General view of Continuously – cooled Lithium Limiter (CLL) proposed for FTU.
(b),(c) view of CLL in FTU lower port window.

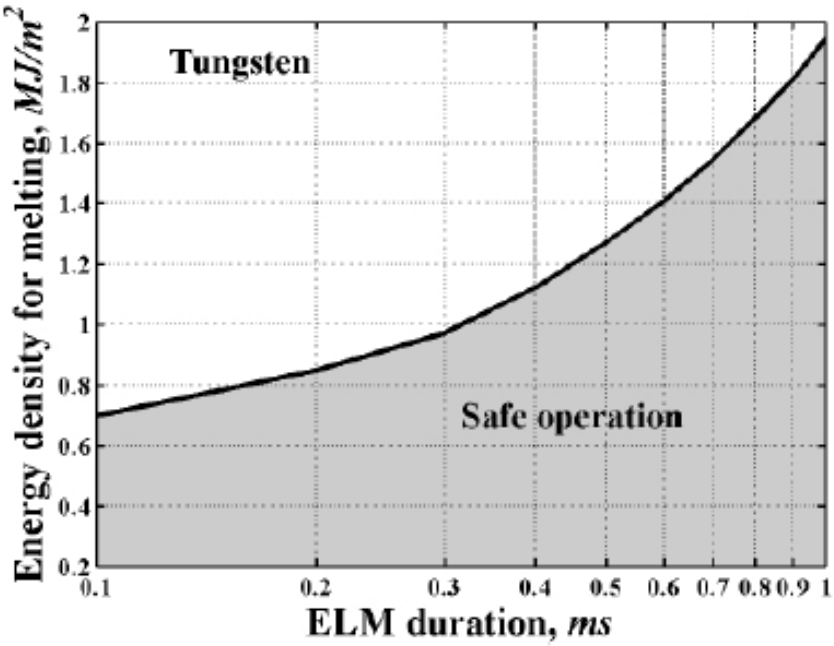

Fig 25: Safe ELM limits for avoidance of melting of tungsten, as predicted in [74].

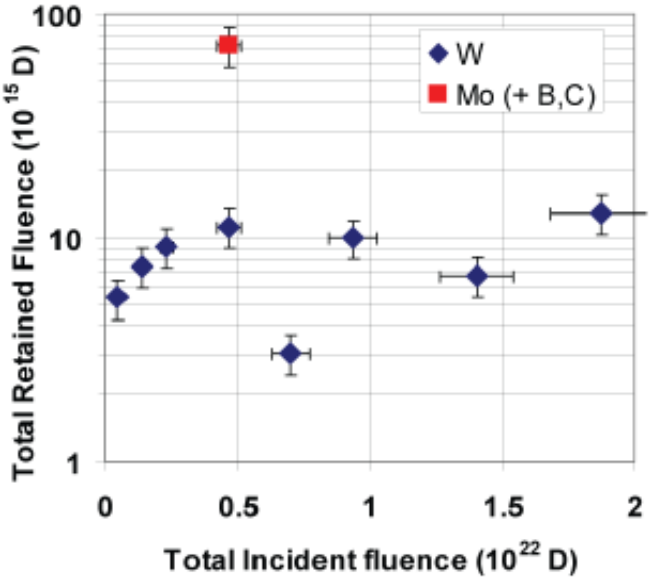

Fig 26: The retained D in tungsten and molybdenum targets as a function of incident fluence [81] in Pilot-PSI tests.

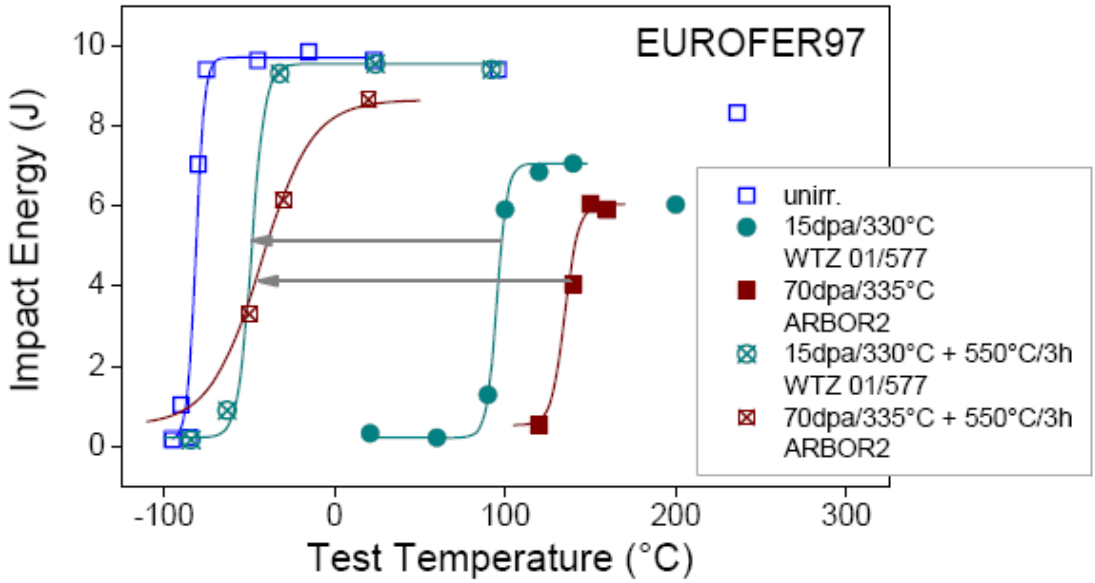

Fig 27: Impact energy vs test temperature for EUROFER from two in-pile irradiations (WTZ 01/577 and ARBOR 2), comparing the as-irradiated condition condition and post-irradiation annealing at 550ºC for 3 hours. Results in the reference unirradiated condition are also shown. Lines are fits to the DBTT, and arrows indicate its recovery.

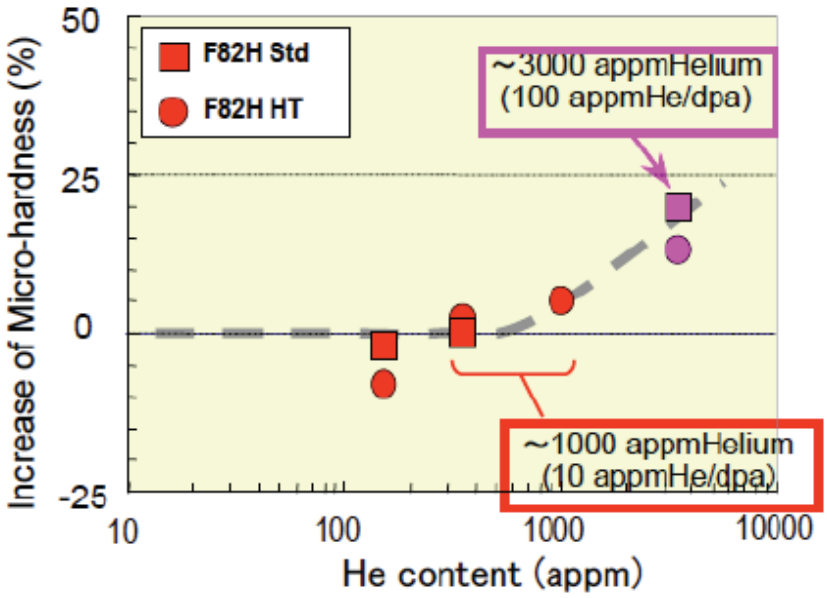

Fig 28: Additional hardening of F82H RAFM steel by helium produced in a dual-beam (Fe and He) irradiation.

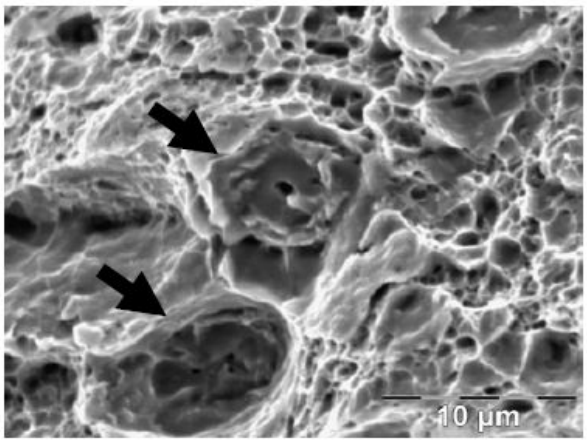

Fig 29: SEM picture of the post-irradiation fracture surface of Eurofer alloyed with micro-quantity (82 ppm) of natural boron "He eyes" features can clearly be seen. (irradiation and test temperatures are 300°C).

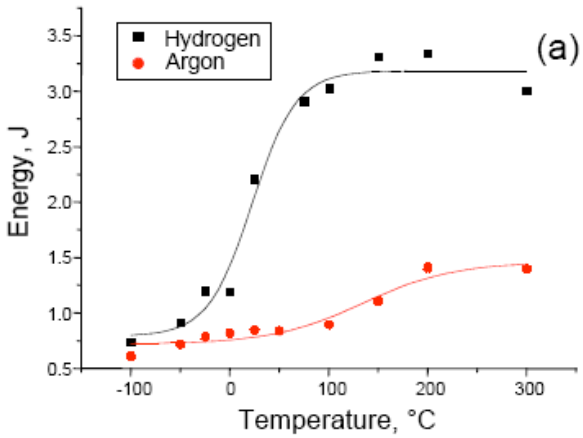

Fig 30: Absorbed energy vs test temperature for Fe-14Cr-2W-0.3Ti-0.3Y_2O_3 ODS steel prepared from powders mechanically alloyed in argon and hydrogen atmospheres.

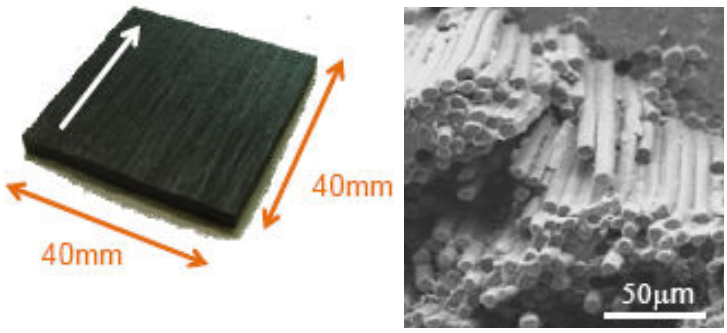

Fig 31: Sample and microstructure of NITE SiC/SiC composite

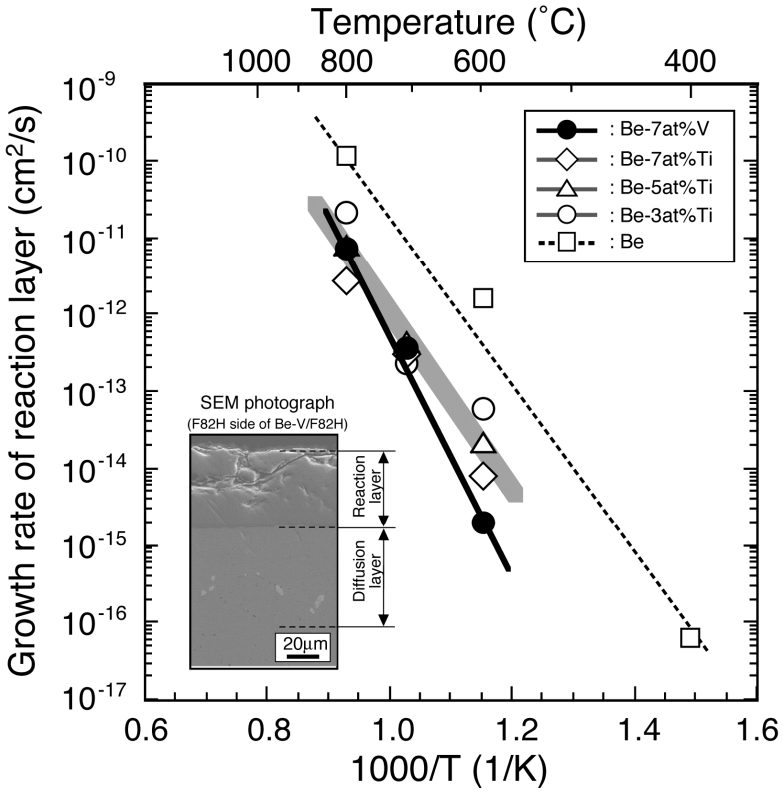

Fig 32: Comparison of growth rate of reaction layer between RAFM Steel (F82H) and pure beryllium and advanced beryllium alloys Be-Ti and Be-V.

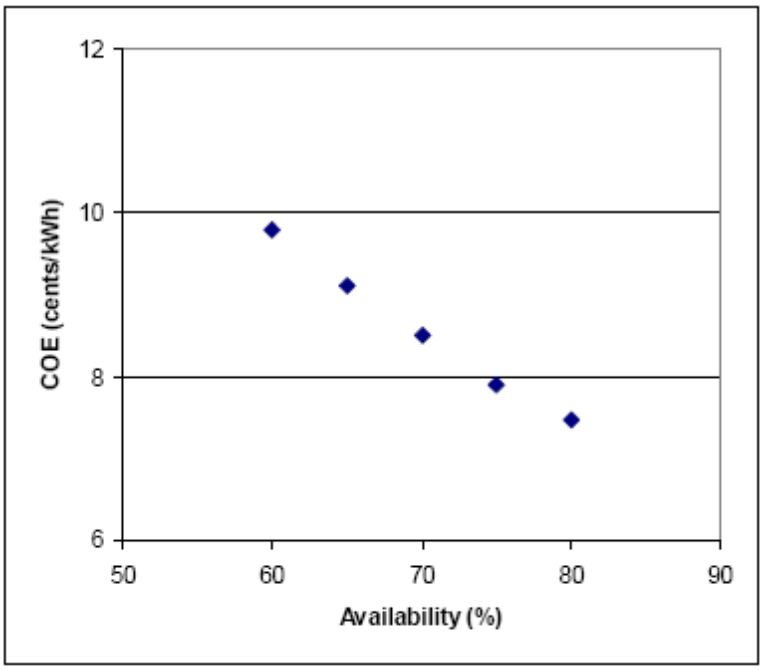

Fig 33(a): Cost of electricity from a fusion reactor concept as a function of machine availability. Here the availability has been fixed, and not allowed to vary in a full optimisation, which would include allowing device size to increase, and concomitant radiation damage to fall.

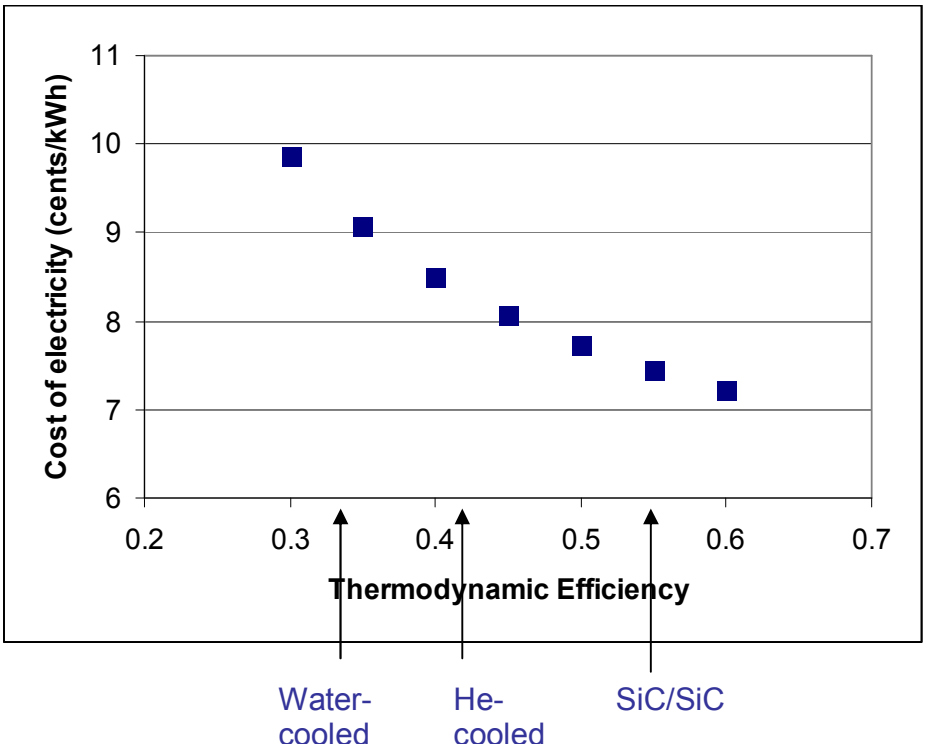

Fig 33(b): Cost of electricity as a function of thermodynamic efficiency of the fusion reactor. In this study the availability is fixed. The arrows indicate the thermodynamic efficiencies for water-cooled and helium-cooled steel blanket designs and for SiC/SiC blanket concepts.

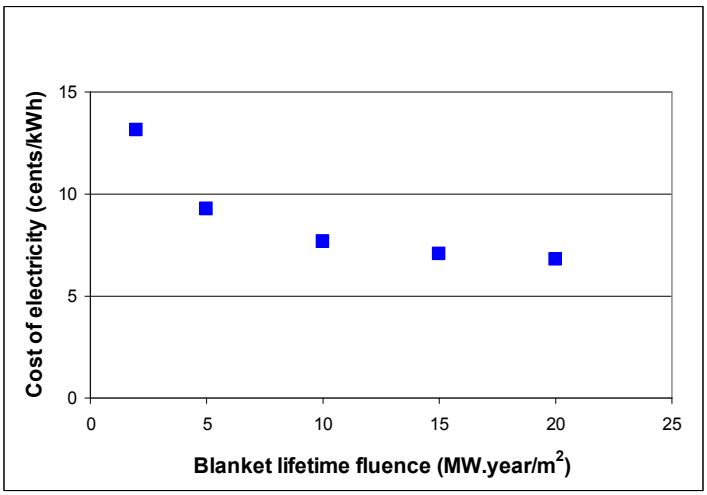

Fig 34: Cost of electricity prediction as a function of the blanket lifetime neutron fluence limit. Fluence is expressed as MW.yr.m^{-2}. For steels, 1 MW.yr.m^{-2} is ~ 10 dpa.